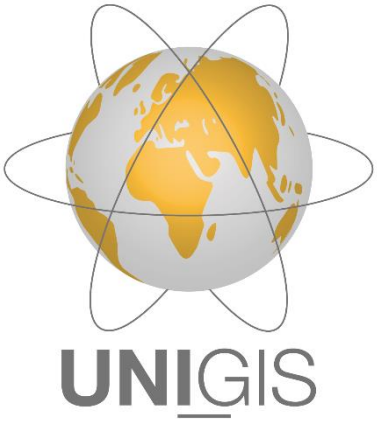

Master Thesis

submitted within the UNIGIS MSc programme
Department of Geoinformatics - Z_GIS
University of Salzburg

Application of SAR Change Detection to Evaluate Flood Event Characteristics Pre and Post Restoration of a Floodplain

by

Sean Jarrett
u106709

A thesis submitted in partial fulfilment of the requirements of
the degree of
Master of Science (Geographical Information Science & Systems) – MSc (GISc)

Advisor:

Dr Daniel Hölbling

Brighton, UK, 7th October 2022

Table of Content

List of Tables and Figures

Abstract

This study proposes an evaluation method using C-band Sentinel-1 synthetic aperture radar (SAR) data to provide evidence of flood characteristic changes after the restoration of a floodplain. A portable, flexible evaluation framework has replicated previous change detection research approaches to analyse a Natural Flood Management (NFM) project on the Sussex Ouse river, conducted by the Sussex Flow Initiative (SFI), to ascertain how control measures have helped alleviate flood risk. GIS operations were conducted on the mapped results of the change detection procedure to identify how flood area, form and compactness have been affected after the NFM installation restored a floodplain to slow river flow and how these changes relate to the overall aims of the project. Innovative means were employed to verify the change detection methodology by sampling flood records from internet-published drone footage. The use of SAR data provides evidence of how NFM features function during significant flood events, providing mapped delineation of flood extent. A comprehensive scorecard has been developed to evaluate the positive and negative outcomes of the spatial changes that have manifested in post-restoration floods, in comparison to inundation before the installation. Results from this study have been included in the annual report of the SFI project to demonstrate how key features have attenuated flood waters in accordance with design intentions.

Acknowledgements

I would like to acknowledge the contributions made to this study by various individuals that have supported me in developing the research. Sam Buckland of the Sussex Flow Initiative enthusiastically embraced the potential that remote sensing offers to the development of NFM and took the time to welcome me on my visit to Cockhaise Brook and respond to my findings and requests. Supporting me with a forensic zeal in proof-reading my drafts have been Suzanne and Pauline Jarrett. Finally, I would like to thank my thesis supervisor Dr Daniel Hölbling for the prompt support, guidance and encouragement that has been provided.

1. Introduction

1.1. Motivation

To meet the challenges posed by climate change, long-term English government investment in flood risk planning is now considering the exploitation of Natural Flood Management (NFM) techniques to slow down and store floodwaters in conjunction with traditionally engineered solutions (Environment Agency, 2020). NFM installations form a key facet in reducing flood risk to achieve policy goals set in the UK 25 year Environmental Plan (HM Government, 2018). Proposals include funding to increase knowledge and learning in the application of NFM techniques.

Currently, very little specific research exists that has evaluated the effectiveness of NFM techniques in positively affecting flood events. A study from 2004 in the USA looked at over 37,000 river restoration projects and could only find 10% that considered any form of assessment/monitoring and 'most of these….were not designed to evaluate consequences of restoration activities or to disseminate monitoring results' (Bernhardt et al., 2005, p.637). This lack of performance monitoring is still evident, which has motivated the development of a strategic approach in monitoring natural infrastructure projects, such as NFM (van Rees et al., 2022). Evidence has been gathered in the UK on the use of natural processes in ecosystem services, which includes river and floodplain restoration. However, there is acknowledgement of a current lack of field-based verification of potential benefits, especially highlighting identification of flood risk management advantages (Environment Agency, 2018).

Bernhardt et al (2005, p.637) implore the use of some sort of assessment to 'enable restoration practioners….to understand what types of activity are accomplishing their goals'. The accessibility and temporal consistency of satellite imagery, such as the Landsat and Sentinel programmes provides a reliable platform from which standardised processes can be deployed to compare relative NFM performance against more intensive flood management interventions.

Remote sensing techniques combined with Geographic Information Systems (GIS), provide the opportunity to evaluate the performance of NFM installations at every scale of their implementation. Passive and active satellite systems can be used to sense water surfaces, including with some technologies through dense vegetation and in challenging weather conditions. Recent research has advocated the use of these resources in measuring performance of nature-based services (NBS), such as NFM (Kumar et al., 2021). This catalogue of data, with global coverage and high temporal resolution provides a rich library from which changes in flood pattern can be analysed. GIS provides the tools to manipulate data to visualise and analyse these changes in relation to how they may affect the landscape in a river or wetland catchment.

1.2. Literature Review

Optical satellite systems passively use reflectance values in the electromagnetic spectrum to sense the Earth's surface to very high temporal and spatial resolutions. Open source multi-spectral imagery from the Landsat and Sentinel-2 optical satellites has been used to combine infra-red, near infra-red and green wavelengths to effectively identify flood waters (Klemas, 2015).

The prevalence of cloud cover is an important consideration when sensing flood events. Whilst this has been extensively addressed in flood inundation studies using spectral imagery (Zhou et al., 2017), Synthetic Aperture Radar (SAR) technology has the ability to penetrate cloud cover (Huang et al., 2018). SAR is an active remote sensing technique that transmits and receives bursts of microwave energy. These received bursts are measured as fractions of the incident energy emitted by the radar and processed as intensity values, referred to as backscatter. Imagery data contains these received intensity values and phase information, which is used to identify land cover features

such as water surfaces and conditions, for example, soil moisture content. The key considerations specified by Kasischke et al (1997) for SAR use in flood detection and wetland monitoring are as follows:

- Microwave frequency: X or C band for open wetlands/floodplains. L or P band for monitoring flooded forests, with some sensitivity at C-band.
- Polarisation: co-polarisation (vertical emittance and vertical return – VV) or cross-polarisation (vertical emittance and horizontal return – VH).
- Incidence angle: low (20 to 40°) and below 20° for flooded forests.
- Spatial resolution: high.
- Sampling frequency: high.

These considerations indicate another important aspect of SAR technology. Where flood extent could be masked by foliage, depending on the wavelength range used, SAR has varying abilities to penetrate vegetation (Huang et al., 2018). Lower frequency P and L band sensors are more suitable for forest canopies. C-band has been found to be more effective in wetlands, where more herbaceous vegetation is prevalent.

Polarisation refers to the geometric plane of the radar wave. Particular configurations have been found to ably detect flooding under vegetation, as the considerations set out above. The orientation of branches and leaves scattering incident energy will have a significant effect on the polarisation of received energy transmissions by the sensor (Kasischke et al., 1997). Manjusree et al (2012) evaluated the detection of water bodies in different polarisations and found VV to have higher sensitivity than VH for surface roughness. Clement et al (2018) proposed that pluvial flooding cannot be detected in VV polarisation, as flooding away from the floodplain was only detected in VH data.

Where there is no surface wind disturbance, the flat nature of water features act as a specular reflector (Carreño Conde and De Mata Muñoz, 2019). Incident energy bounces off the surface at an angle (forward scatter), diverting away from the satellite sensor. Water bodies are therefore represented as dark, almost black features. Whereas, the multi-directional scattering and attenuation of incident energy caused by land features such as trees and vegetation will return a greater proportion to the sensor (backscatter) and display more brightly. SAR flood detection techniques rely on the recognisably low backscatter characteristics of water surfaces to delineate areas of inundation. Carreño Conde and De Mata Muñoz (2019) generally found water surface backscatter intensity values below -20dB. Manjusree et al (2012) identified flood water intensity values ranging from -6 to -24dB.

Surface roughness of vegetation and forests will result in strong backscatter intensity in comparison to water. A flood situation though presents the scenario whereby the presence of water can, depending on the vegetation type, actually increase intensity due to a double bounce effect from the flood surface below (Kasischke et al., 1997). However, the forward scattering of inundated wetland terrain without the denser cover provided by trees, actually reduces the radar backscatter. This has been observed in wetland marshes, where sparser vegetation cover produced decreased backscatter magnitudes (Kasischke et al., 1997). Extensive investigations by Zhang et al (2022) has identified the effect water depth has on C-band backscatter in vegetation, where over a certain depth energy starts to forward scatter.

SAR intensity measurements can also be affected by radar shadow and foreshortening. Shadow effects are caused by more rugged terrain or high buildings. Foreshortening and layover effects are

the result of the incidence angle and range of the SAR technology used. Using images on the same orbit negates these effects during analysis (Cian et al., 2018).

There is also a seasonal dimension to consider with all remote sensing applications. For SAR, Martinis and Rieke (2015) found seasonal freezing affected the variability of backscatter returns. In summer, it has been found that water in marshland acts as a corner reflector, resulting in higher backscatter values. The growing seasons affect the sensitivity of agricultural land, where there can be reduced clarity in winter compared with water (Cihlar et al., 1992). Martinis and Rieke (2015) also found there to be a large variance in agricultural land over the phenological cycle, in addition to soil moisture changes and even furrow orientation. Seasonality plays a major role in how flood inundation is detected. Schlaffer et al (2015) highlight the difference between land where the dielectric constant (the electrical characteristic measurement of a surface) gradually increases with rises in soil moisture during wet seasonal periods and sudden change to dry land. A greater drop in backscatter intensity is experienced in the latter scenario.

These changing characteristics of surface features led Martinis and Rieke (2015) to conclude that empirically defined thresholds cannot be used to detect flood waters. They proposed the inclusion of fuzzy logic-based algorithms and change detection as a means to achieve more stable threshold settings from which to detect flood waters. Change detection also lends itself well to scenarios where temporal comparison of SAR images is used to detect flood waters (Brivio et al., 2002).

Change detection presents the opportunity to exploit the use of easily accessible SAR imagery with global coverage to detect flood waters with temporally significant imagery around a flood event. This form of remote sensing analysis can be described as 'the process of identifying differences in the state of an object or phenomenon by observing it at different times' (Singh, 1989, p989.). Green et al (1994, p331) highlighted the fundamental requirement of 'controlling all variances caused by differences in variables that are not of interest'. This requires that all variances other than the variable of interest, in this case land cover, are as far as possible constrained. Using the same data source and processing specifications, allows the focus of variability to be concentrated on changes to backscatter in relation to a flood event. The availability of suitable data will be dictated by flood event occurrence dates, budget restrictions and in application to the evaluation of where flood management measures have been introduced, identifying flood events pre and post-installation that are seasonally aligned (Munyati, 2000). There is also the trade-off between budget and spatial resolution that will impact on the overall accuracy potential (Lu et al., 2004). As outlined above, phenological and seasonal variance needs to be minimised as much as possible in change detection (Lu et al., 2004). Clement et al (2018) chose to apply a secondary threshold to overcome seasonal variation, using a global threshold for land-water delineation.

To provide meaningful insight, Lu et al (2004, p2368.) identify four sets of information that should result from change detection analysis:

- 'Area change and change rate'
- 'Spatial distribution of changed types'
- 'Change trajectories of land-cover types'
- 'Accuracy assessment of change detection'

Lu et al (2004) review a multitude of different change detection techniques in remote sensing and GIS application. The algebraic technique of image differencing only identifies the dimension of change/non-change. Whilst easy to understand, threshold values are difficult to establish. Standard deviation provides a balanced threshold value, but will not be suitable if there is any imbalance in

change values. Kappa analysis should therefore be used to determine the suitability of the threshold values ultimately used (Macleod and Congalton, 1998). Principal Component Analysis (PCA) transforms raw data values of two datasets to highlight otherwise hidden differences. Knowledge of the backscatter characteristics of the classes to be analysed and again threshold settings are fundamental to preserving accuracy (Macleod and Congalton, 1998). Post-classification is a change detection technique that as its name suggests executes a comparison of multi-temporal datasets after a classification process has been conducted and hence needs no further classification to identify further change information. Whilst elementary, the number of steps in a post-classification process do risk introducing inaccuracies. Image differencing and PCA have the advantage of restricting error potential by classifying areas of change only and requiring specific reference data (Macleod and Congalton, 1998).

Matgen et al (2011) found that a simple change detection process using manual threshold selection achieved comparable results to a more sophisticated process involving a probability density function stage to identify optimum thresholds and region growing to delineate homogenous areas of water bodies. Root mean square error (RMSE) in terms of pixels, for each method respectively was 1.29 and 1.27. Essentially, the identification of a suitable change detection method centres on the specificities of a study and is heavily influenced by analyst experience with a particular method. The use of combined techniques has also been employed to improve results (Lu et al., 2004).

A change detection approach based on statistical analysis of a large set of reference images to obtain a comprehensive understanding of the backscatter variance within an Area of Interest (AOI) yielded spatial agreement of 97% (Cian et al., 2018). This method provides the ability to build a statistical profile of flood events before and after the installation of NFM measures on a river catchment and uses the threshold coefficients developed by Long et al (2014) in a method termed change detection and thresholding (CDAT).

CDAT can also be utilised to compare flood events. This uses image differencing and a decision-based thresholding process to produce spatial agreement of between 89 and 92% against Landsat classification (Long et al., 2014). A very similar CDAT method proposed by Clement et al (2018), produced a Kappa statistic of 0.778 in VH polarisation and 0.799 in VV. Decision-based thresholding involves a series of specified steps that mask certain pixels not meeting specific criteria to minimise possible misclassification and set a threshold for the remaining dataset based on the mean difference value and the standard deviation. Maximum slope (Long et al., 2014) and height above nearest drainage (HAND)(Clement et al., 2018) have been used as criteria to minimise misclassification where flood waters will not accumulate.

The CDAT method of Long et al (2014) has an elementary approach that can be easily automated. It can also be flexibly applied to most areas of interest, including the use of SAR with different incidence angle.

The Sentinel-1 satellite system uses C-band microwave frequency. The incidence angle range in the Interferometric Wide (IW) swath mode is 29.1 to 46°, with the dual options of co-polarisation (VV) or cross-polarisation (VH). Level 1 Ground Range Detected (GRD) IW products have a 10x10m resolution. Temporal resolution is 12 days. The practical consideration of acquisition cost also has to be included with these requirements, as the Sentinel programme provides open access to datasets.

Pre-processing of data is an important procedure in any remote sensing application. For change detection, the exact replication of selected parameters for multi-temporal viewpoints, such as image registration, is of paramount importance. Along with this comes radiometric correction, which needs

to be consistently applied to all datasets used (Lu et al., 2004). A rapid flood mapping process proposed by Bioresita et al (2018) uses sigma-nought radiometric calibration, citing better water/land separation in statistical tests.

To provide further context to SAR imagery, local historical meteorological records such as precipitation, air temperature, soil temperature and wind conditions can help interpret imagery data (Cihlar et al., 1992). Local river records are also important in mitigating the lag between the flood peak and the satellite pass. Reducing this lag as much as possible is crucial in mapping the full extent of the flood (Brivio et al., 2002).

Historically, a fundamental barrier to the use of SAR data was the existence of speckle interference in an image (Kasischke et al., 1997). Extensive research analysis and the resulting processing technology generated, provide a sound basis from which to select a suitable filter in particular applications of SAR remote sensing. Criteria used to reduce speckle noise has considered the specification of SAR system used, conditions during image acquisition and terrain to determine the type and sequence of filter to be applied. Conde and De Mata Muñoz (2019) decided on the Lee filter using a 7 x 7m window. Bioresita et al (2018) assessed a range of filter options and elected to use a Median filter with a window size of 5 x 5 pixels. This was also used by Clement et al (2018) for their flood mapping change detection study. For a TerraSAR-Z image detecting flooding on the River Severn in England, Martinis et al (2009) used a 3 x 3 pixel Gamma MAP filter, due to its relative computational efficiency and the cited quality of results generated. This is supported by the findings of Manjusree et al (2012) and was also used by Long et al (2014). An evaluation of speckle filtering algorithms based on C-band RADARSAT imagery for flood delineation, also found the Gamma MAP filter, with the same window size, achieved the best results based on mean square error (MSE) and signal-to-noise ratio (SNR) ratio and was comparable using the speckle suppression index (SSI) against the Lee and Frost filters (Senthilnath et al., 2013). It should be noted though that the effects of speckle filtering are a reduction in image resolution and changes to pixel values depicted as speckle. This therefore provides the potential for misclassification of flood water pixels (Liang and Liu, 2020).

Ground truth records are required to verify flood extent in order to produce a comparable accuracy assessment. Unless reliable records have been kept of the flood extent, ground truth data with suitable spatial resolution has to be sourced. The remote AOI in Namibia studied by Long et al (2014) required the use of Landsat 8 Operational Land Imager (OLI) imagery. Clement et al (2018) compared SAR detection with Sentinel-2 optical imagery and modelled 100 and 1,000 year event extents produced by the UK Environment Agency.

Whilst research exists that seeks to evaluate the installation of various NFM measures, focus has been on the use of hydraulic modelling or ground-based monitoring to assess performance in flood situations (Iacob et al., 2014). Key factors to be considered include the main objectives of the NBS, performance criteria, elements affecting NBS performance, suitable available data and practical monitoring scale (Kumar et al., 2021). There are no internationally-recognised monitoring standards for NFM or the wider domain of NBS. Indicators can be objective or subjective in focusing on the overall project goals and are usually identified during the initial design stage of the NBS installation. Project management principles apply in ensuring that indicators are SMART (simple, measurable, achievable, relevant and time-bound).

Budget is key to how monitoring is incorporated through modelling, new ground-based sensor technology or remote sensing. There have been studies promoting the use of remote sensing in monitoring performance of NBS installations after fluvial floods at catchment scale, due to their

extensive geographic coverage, cost effectiveness in most circumstances and the ability to produce data in poor weather conditions (Kumar et al., 2021).

1.3. Problem Definition

This study proposes the use of remotely sensed satellite imagery to support and enhance the evaluation of NFM installations. Change detection provides an accurate and effective methodology to detect the effects on spatial form of inundation in a riverine region during events before and after NFM floodplain restoration. Most NFM projects are smaller-scale, community-driven initiatives that have piloted approaches that augment and, in some cases, provide an alternative to traditionally engineered flood solutions. The philosophy therefore in undertaking this study has been to use only open-source data and software. This will help strengthen the portability of this research for use in evaluating other flood management projects that have not considered how remote sensing can be used to evaluate inundation performance.

1.4. Aims and Objectives

The aim of this study is to apply SAR change detection to provide an evaluation of the effects of floodplain restoration on the characteristics of flood events before and after restoration. Evaluation will assess the overall spatial effect on the river catchment in question and in specific relation to the floodplain restoration and other less prominent NFM installations employed. The objectives are set out as follows:

1. A suitable restoration project will be selected that has used NFM measures on a floodplain to attenuate floodwaters and identify project goals of beneficial changes to flood characteristics.
2. Open-source SAR imagery for comparable flood events pre- and post-restoration will be selected in terms of seasonality, river level records and weather conditions affecting SAR sensitivity.
3. An accuracy assessment will be undertaken to verify how the method of change detection of flood waters performs in relation to known areas of inundation using identified ground truth samples.
4. These change detection procedures will be employed to delineate differences in flood extent, form and compactness across the catchment area for assessment against the specific project evaluation criteria.

2. Methodology

The aim of this study was to evaluate the effects of a natural flood management (NFM) installation on the Cockhaise Brook tributary of the Sussex Ouse river. Change detection and thresholding (CDAT) of remotely sensed SAR satellite imagery was employed with the image difference technique to detect flood waters and inundated vegetation. Most NFM projects have been developed by third sector environmental organisations on limited budgets, where resources for evaluation of results have historically been limited or non-existent. Open data sources and software have therefore been deliberately chosen to develop an evaluation process that could be employed on similar projects in the future.

Two temporal sets of data were compiled to represent pre- and post-NFM installation floods, allied with a baseline reference image when the river was at a seasonally-similar average level for each event. These datasets were based on comparable flood peaks, to evaluate how the flood inundation may have changed in the vicinity of the NFM measures.

Research objectives followed defined change detection principles (Lu et al., 2004) by focusing on:

- Detected flood area change. With comparable flood peaks being assessed, the effectiveness of the NFM installation was evaluated in relation to whether the overall area of flooding had changed.
- Spatial distribution of change in detected flood. Changes in spatial form of the post-NFM flood in comparison to how Cockhaise Brook previously flooded, with a focus on possible spatial relationships between the post-NFM detected flood form and the position of the NFM features.
- Accuracy assessment. Accuracy of the change detection technique used was verified by applying the same methodology to satellite imagery on areas of the Ouse or other local rivers where known flooding occurred on specific dates, for use as a ground truth reference. Reliable local anecdotal evidence was also used to create spatial records of known flood and ‘dry’ areas around the NFM features to augment these references.

2.1. The Study Area

The Sussex Ouse is a lowland river system running through the Weald geology of clay and sandstone, before cutting through the chalk downs around the town of Lewes and flowing into the English Channel at Newhaven. Cockhaise Brook is approximately 8km long and connects with the Ouse in relatively more hilly terrain through a more varied geological landscape of Wadhurst clay and the start of the High Weald sandstone.

The Sussex Flow Initiative (SFI) is a multi-agency project that has installed NFM measures in the Ouse catchment to reduce flood risk by re-engaging the floodplain. The main measures are situated at Woodsland Farm, near the market town of Haywards Heath in West Sussex, with the area of interest (AOI) a series of features on Cockhaise Brook. These were introduced to reduce local flood risk around the now-residential Cockhaise Mill area. A map of the Cockhaise Brook AOI is shown below in Figure 2.1.1.

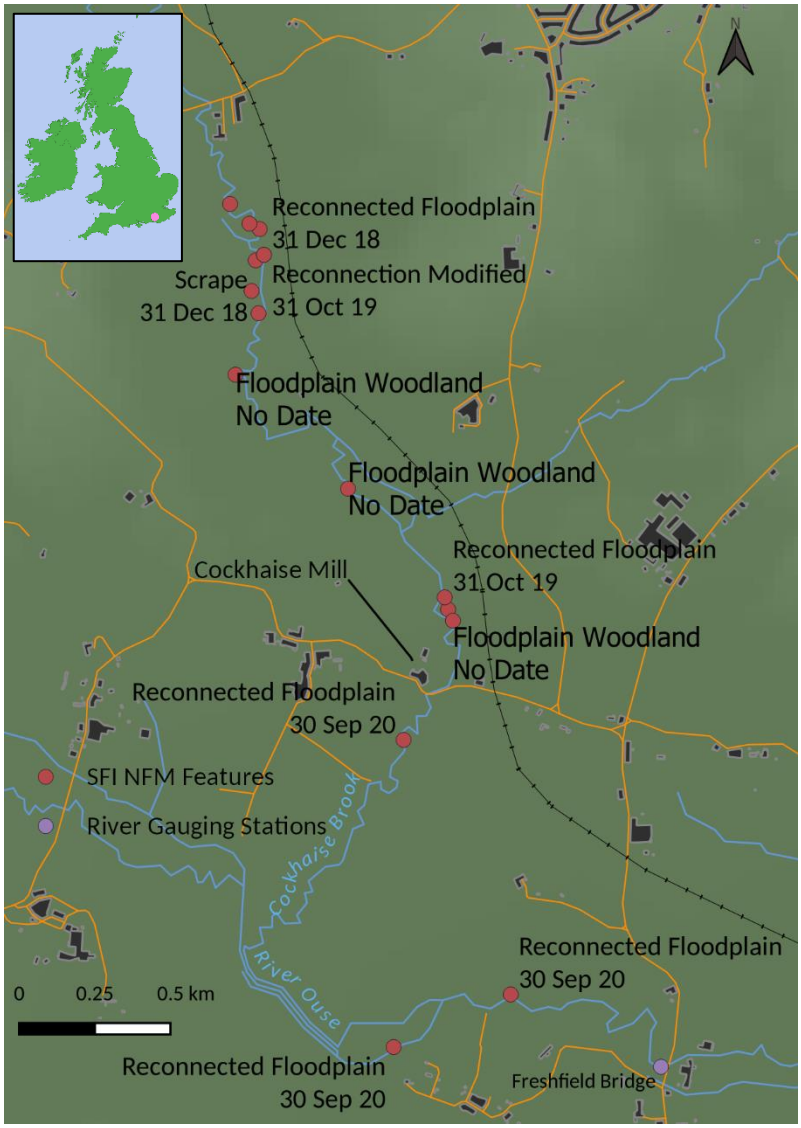

Figure 2.1.1: *The Cockhaise Brook AOI including installed NFM features.*

The main measures installed were two 'Run-off Attenuation Features' (RAFs), more commonly referred to as scrapes, both approximately 500m2 in area. Figure 2.1.2 below shows a photograph of the primary scrape, partially flooded in early spring. The evaluation has provided evidence as to how these scrapes attenuate water during a substantial flood, the effect on the brook catchment immediately up and downstream of the scrapes (a study area of approx. 9km^2) and most importantly if flood extent around the mill has changed and how.

Figure 2.1.2: *The primary scrape installed on reconnected floodplain adjacent to Cockhaise Brook to attenuate flood waters.*

2.2. Change Detection

The principles of change detection require the controlling of all possible variances (Green et al., 1994). Therefore, C-band SAR imagery from Sentinel-1 (S-1) satellites with the same specification was acquired to represent two scenarios; a specific fluvial flood event and a baseline snapshot of seasonally low river flow. Records from the closest downstream gauging station were used to identify similar river levels for flood and reference dates before and after the NFM installation and for a ground truth flood event. Nearby weather records were also consulted, to ensure the wind conditions of the flood and reference images were as closely aligned as possible, as this may have an effect on the satellite backscatter for open water.

Image differencing change detection formed the basis of the study approach. This is a simple technique that can be easily implemented using open-source data such as S-1 imagery. The CDAT method established by Long et al(2014), has demonstrated between 77 and 91% agreement with Landsat flood classification and has been used in situations where there is a lack of ground truth data. As the SFI NFM project is quite small-scale, accurate local flood records had not been kept by agencies. This, along with persistent cloud cover during periods of flood susceptibility, make it difficult to use optical satellite imagery, such as Landsat.

2.3. Data Acquisition

The first Sentinel-1 images became available after the launch of the satellite on 12th April 2014. A pre-NFM data extent was therefore set from this point until before the first NFM features were installed in December 2018. The temporal window for post-restoration data was from October 2019 (the installation date of the final NFM feature) onwards.

Selection of comparable datasets, capturing the river in a seasonally benign state (baseline) and during the peak of a flood event (flood) was based on specific criteria to control all input variables, as necessitated by change detection principles. The criteria takes into account:

- the satellite mission (1A or 1B)
- the pass time (ascending or descending)
- wind conditions and direction

Wind conditions have the potential to influence backscatter values on flood waters through surface ripples/waves acting to disperse radar waves rather than act as a specular reflector (Manjusree et al., 2012).

The Gold Bridge gauging station, situated approximately 13km downstream of the main NFM features, is the nearest data source for river flow volumes. For river level records, the Freshfield Bridge gauging station, only 6km downstream, provides a more accurate basis for determining peak flood levels for the AOI. Although this was augmented with the Gold Bridge flow records.

From the UK National River Flow Archive, the highest peak flow recorded at Freshfield Bridge since the NFM features were installed was 67.69m^3 per second on 20th December 2019. A S-1A descending image was captured at 6am on this date, which provided data at the greatest peak of the flood. Media interest in this sizeable flood event, provided more leads in researching records upon which ground truth datasets could be formulated.

River level records at Freshfield gauging station for the pre-NFM period from when S-1 imagery first became available were analysed first, to identify the largest flood peak from which to map inundation before management measures were in place. The highest level recorded was 2.12m (daily average 1.75m) on 11th January 2016, with the fourth highest the day before measuring 1.6m. The blue zone illustrated in Figure 2.3.1 below illustrates the short peak window in which SAR imagery could be used (10th to 13th January 2016). A baseline date could be selected from the period shown in green, where the river was at consistently low levels.

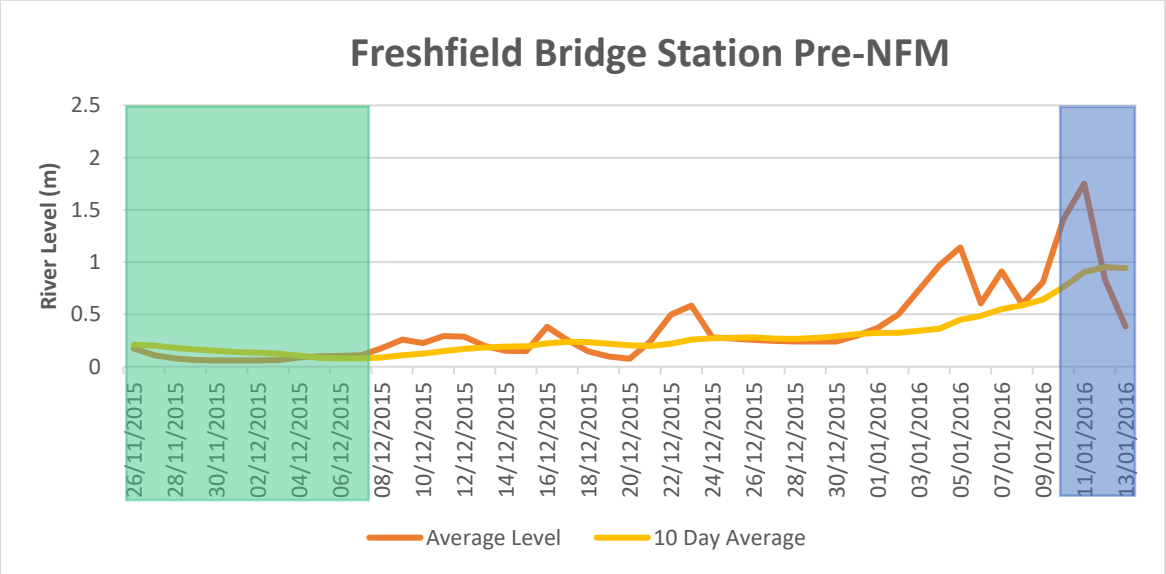

Figure 2.3.1: *Daily average levels recorded at the Freshfield Bridge gauging station on the Sussex Ouse for the period around the highest flood peak between the launch of S-1 satellites and the installation of NFM measures on Cockhaise Brook.*

S-1A imagery capturing the AOI at a pre-NFM flood peak was available on 10th January (fourth highest recorded level) in a descending pass and 13th January in an ascending pass (recorded level 0.45m compared with the 1.75m peak on 11th January). Both of these dates had potentially different insights into the flood: 10th January provided the fourth highest recorded level; 13th January a snapshot of flood waters that would have more slowly permeated through the clay substrate surrounding the NFM measures. Local weather records show relatively strong south easterly wind speeds of 35 and 22km/h respectively, on both of these dates.

Table 2.3.1: *Summary of key data for the selected flood and dry dates for the pre-NFM change detection operation.*

Satellite Specification	Flood Date	Dry Date	Wind Speed/ Direction	Mean Flow m3/sec at Gold Bridge (5 yr av = 2.05)
1A 6am descending pass	10th January 2016		35km/h SE	19.80
		5th December 2015	41km/h SE	1.81
1A 6pm ascending pass	13th January 2016		22km/h S	6.64
		26th November 2015	15km/h SW	2.04

Table 2.3.1 above shows the compatibility of the selected images representing a baseline state against the flood event datasets, with like satellite specifications and wind conditions. Reference has been made to the average flow recorded at Gold Bridge, to provide greater context as to the size of the flood on the Sussex Ouse.

The highest post-NFM flood level recorded at Freshfield Bridge was 2.68m (daily average 2.31m) on 20th December 2019. To put the magnitude of the flood into context, the highest ever daily average level recorded at the station was 2.63m in January 2008. As no comparable pre-NFM flood exists, data around this date, illustrated in purple in Figure 2.3.2 below, could only be used for analysis of local ground truth sites to assess accuracy.

The next largest post-NFM flood occurred on 27th November 2019 and at 2.14m (daily average 1.77m) was almost exactly the same level as reached in January 2016. Suitable dates around this peak are shown in blue in Figure 2.3.2. Potential baseline data periods are shown in green.

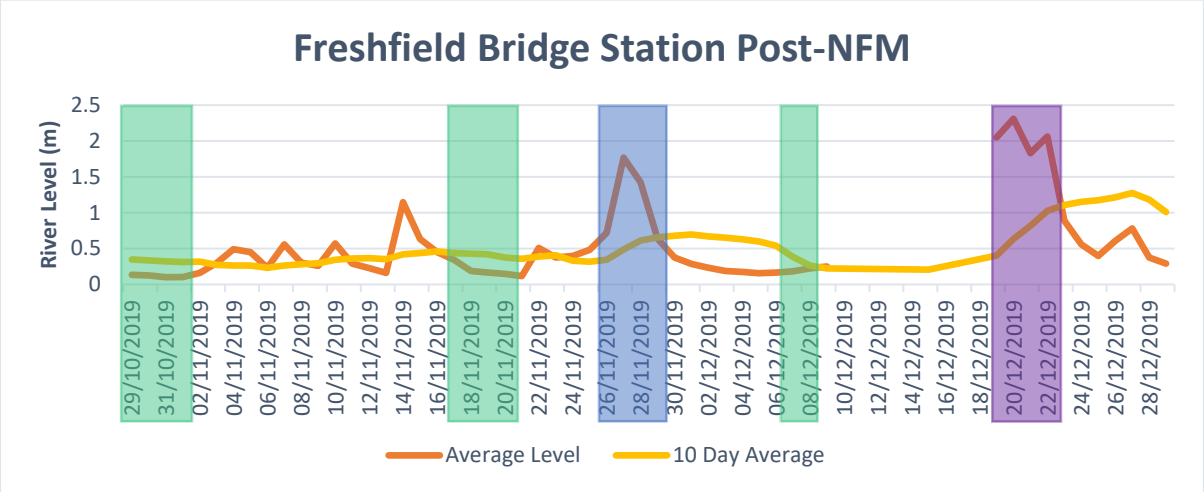

Figure 2.3.2: *Daily average levels recorded at the Freshfield Bridge gauging station on the Sussex Ouse for the period around the highest flood peak post installation of NFM measures on Cockhaise Brook.*

S-1B imagery in a descending pass across the AOI was available on 27th November 2019, capturing the peak of the flood event. Local weather records show very strong easterly wind speeds of 64km/h on this date.

Table 2.3.2: *Summary of key data for the selected flood and dry dates for the post-NFM change detection operation.*

Satellite Specification	Flood Date	Dry Date	Wind Speed/ Direction	Mean Flow m3/sec Gold Bridge (5yr av = 2.05)
1B 6am descending pass	27th November 2019		64km/h E	28.48
		9th December 2019	57km/h S	2.88

For the post-NFM flood, identifying a suitable baseline date in similar wind conditions required that data from after the event had to be selected. The compatibility of the selected datasets can be seen above in Table 2.3.2 in terms of satellite specification and wind conditions for 9th December 2019, as a baseline for the flood event of 27th November 2019.

To remove the possible effects of shadow in elevated areas producing false positives, hilly terrain was masked using a Digital Elevation Model (DEM) dataset (Clement et al., 2018). Replicating the parameters used by Long et al (2014), a mask removing slope over 3 degrees was applied to the S-1 datasets. The most detailed open-source data available was found to be the STRM 1 Arc-Second Global DEM dataset, with a 30m resolution. This was acquired from the USGS online portal, from which a slope layer was derived with QGIS software and a mask created for cells with a slope of less than 3 degrees.

2.4. Pre-Processing Procedures

Europe enjoys ubiquitous coverage of S-1 data in both ascending and descending passes in Interferometric Wide (IW) mode, with dual polarisation. C-band wavelength radar waves are therefore emitted in vertical polarisation and the backscatter responses recorded in vertical or co-polarisation (VV) and horizontal or cross polarisation (VH).

IW mode S-1 datasets have a 250km width, based on three sub-swaths and 5 x 20m resolution. S-1 Level 1 Ground Range Detected (GRD) data products were acquired for the study, with a high-resolution setting. Prior to release, these datasets had been multi-looked and projected based on the Earth ellipsoid model.

Pre-processing of the GRD datasets was carried out using the European Space Agency (ESA) SNAP software, based on the following specification:

- Orbit State Vectors (OSV)
  - The recommended SNAP parameters of Sentinel Precise OSVs and 3rd polynomial degree were used. This process improves the geographic accuracy of the image (Bioresita et al., 2018).
- Removal of thermal noise
- Calibration
  - GRD pixel digital numbers (DN) were calibrated to Sigmaθ values, which have been found to provide the best separation between water and land (Bioresita et al., 2018).
- Terrain Correction

- The STRM 1 Arc-Second DEM dataset was referenced to adjust Sigmaθ values to geocode the image using bi-linear interpolation of the DEM values and nearest-neighbour resampling to the S-1 image.
- Pixel resolution was 10m azimuth x 10m range.
- A WGS 84 geographic projection was used for the terrain correction.

- Speckle Filter
  - Other SAR flood detection studies have extensively tested how different speckle filters used in the pre-processing stage affect flood detection capabilities. To maintain consistency with the methodology used by Long et al (2014), the Gamma MAP filter was applied to the GRD dataset.
  - The Lee filter has been proved to reduce the occurrence of 'false positives' (Carreño Conde and De Mata Muñoz, 2019) and was tested against Gamma MAP.
  - As the AOI is very small in comparison with other change detection research, a 3x3 filter size was used.

2.5. Change Detection GIS Workflow

After pre-processing in SNAP, the raster sigmaθ datasets of dry and flood images were manipulated and analysed in QGIS as the workflow shown in Figure 2.5.1 below.

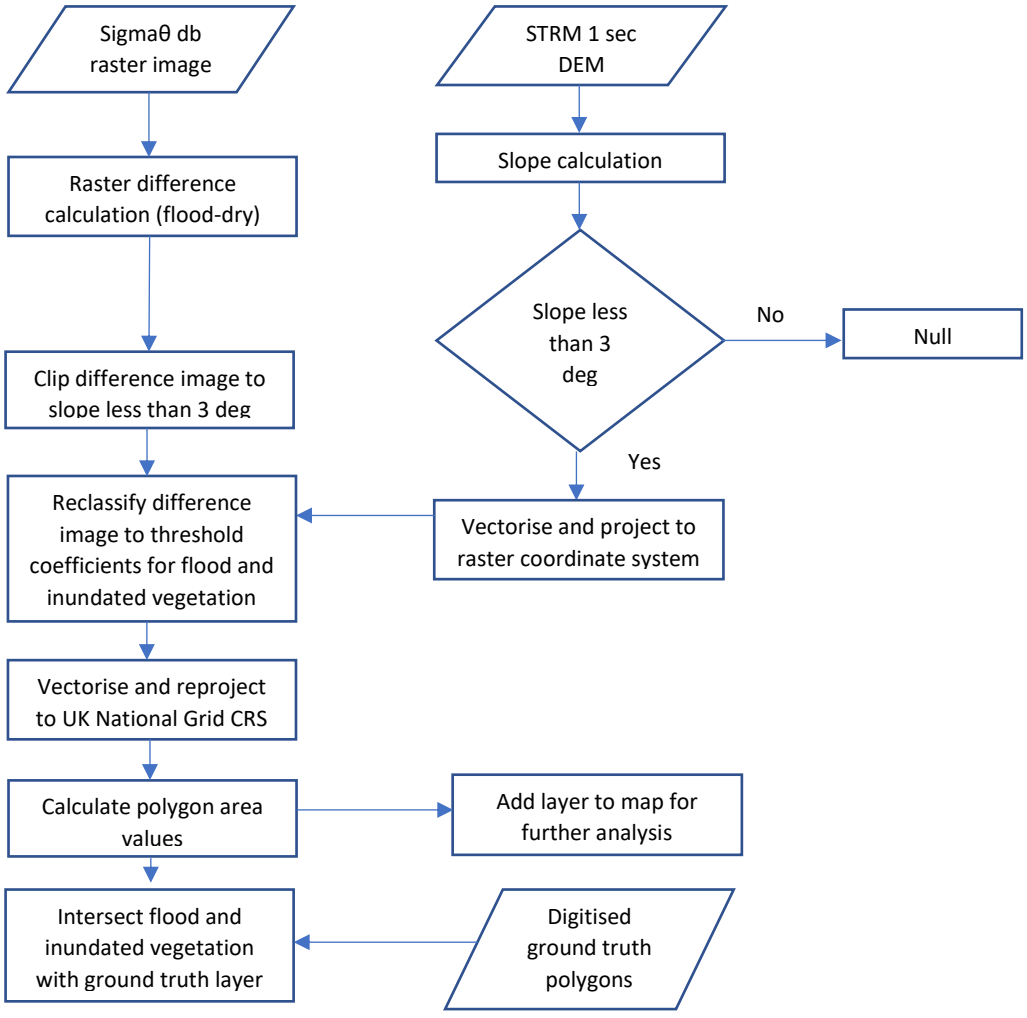

Figure 2.5.1: *GIS flood inundation change detection workflow.*

To undertake the change detection image difference technique, the QGIS raster calculator tool was used. A new raster layer of the difference between the flood and dry values was created and clipped by a mask layer of all slopes less than 3 degrees. The mean and standard deviation values from the resulting masked image difference layer where slope was less than 3 degrees, were then used to formulate histogram thresholds. These thresholds defined open flood water and inundated vegetation pixels, identifying inundation extent.

2.6. Histogram Thresholding

A formula as below, devised by Long et al (2014), was applied to the Sigmaθ dB difference of flood minus reference values, to classify open flood water pixels (P_D), where $lmean$ and $l\sigma$ are the mean and standard deviation respectively of the difference image that has been masked with the layer of sloped surfaces of less than 3 degrees and k_f is the coefficient value.

$$\boldsymbol{P_{D<(\{lmean[D]\}-k_{f*\{l\sigma[D]\}})}}$$

All pixel values below the difference between the pixel mean and the standard deviation, multiplied by the selected k_f coefficient for open flood water are classified as flooded.

The threshold formula to identify inundated vegetation is as the formula below.

$$\boldsymbol{P_{D>(\{lmean[D]\}+k_{f*\{l\sigma[D]\}})}}$$

Here, all pixel values above the sum of the mean and the standard deviation, multiplied by the selected k_f coefficient for inundated vegetation are classified as such.

Threshold values were therefore defined that slice the tails of the overall image difference histogram into detected flood waters and inundated vegetation, as depicted by the orange lines in Figure 2.6.1 below for the 21st December 2019 flood and the reference date of 20th November 2019. The use of the image dataset mean (shown by the red line) and standard deviation (shown by the green lines), ensures that these thresholds are 'sensitive' to the land cover depicted, making this method applicable to most landscapes (Long et al., 2014).

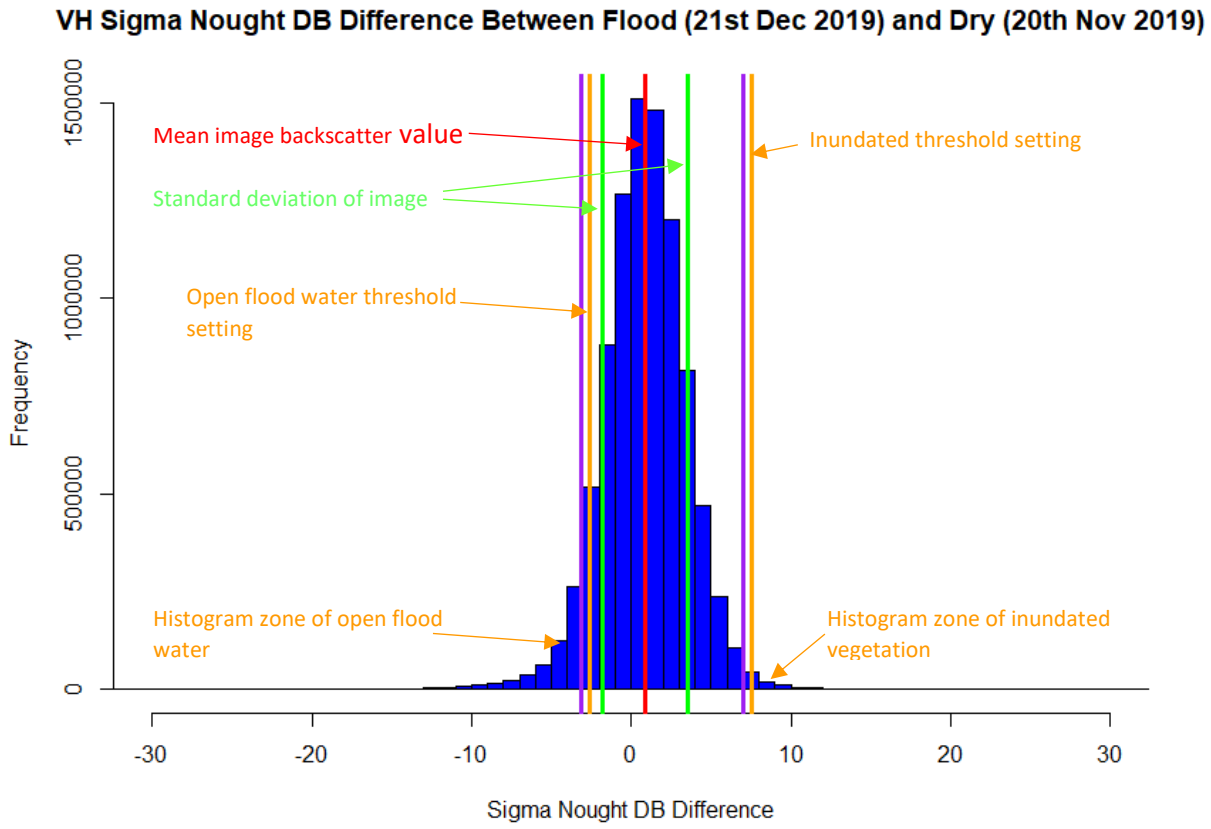

Figure 2.6.1: *Histogram of Sigmaϑ dB values for the difference between the flood image of 21st December 2019 and dry image of 20th November.*

For detected flood waters, these thresholds identify changes in radar backscatter where, in the baseline image, there was surface roughness depicting, say vegetation. In the flood image, these areas produce very low backscatter values, due to the submerged land acting as a specular reflector. The resultant large negative differences in Sigmaθ dB values therefore indicate a change in state from possibly vegetated land cover to flood conditions.

Conversely, the detection of inundated vegetation is achieved by identifying Sigmaθ dB values that have increased due to the reflecting effect of water below the herbaceous cover increasing the scattering of radar waves. It has been found though that under a certain depth of cover between the vegetation and the water line, Sigmaθ dB values start to decrease as the vegetation becomes less disruptive in scattering reflected radar waves (Zhang et al., 2022).

As previously stated though, these anticipated responses of open flood water and inundated vegetation need to be considered in context to the effect of wind on landscape surfaces. Local weather records provide a reference from which compatible temporal datasets have been selected. However, wind direction and gustiness may have a further disruptive effect on the desired compatibility that cannot accurately be predicted.

2.7. Ground Truth Sampling

The assessment of accuracy was based on the use of ground truth sample sites with the following characteristics:

- predominantly natural surfaces, to replicate the landscape around the SFI project.
- in terrain with a slope of less than 3 degrees.
- a cohort depicting flood reference sites that may be susceptible to fluvial inundation, but that are not permanently flooded. The chosen CDAT method is reliant on seasonally similar dry and flood datasets to limit the effect of change due to the agricultural cycle.
- a cohort depicting dry reference sites that even in high magnitude events do not flood.

These ground truth sites need to be relatively large and ideally situated around the Sussex Ouse catchment in order to be relevant to the AOI at Woodsland Farm. The SFI Project Manager S. Buckland provided areas around the AOI that anecdotally do not flood. However, these alone were not of large enough extent to provide a reliable accuracy assessment.

Extensive investigations were carried out involving media coverage searches, contact with local journalists, examination of flood records held by parish, district and county councils and those of the Environment Agency and Fire Brigade. The flood records that were obtained either provided areas highlighted only as at risk or road locations that were not accurate enough to reliably ascertain flood extent. From a temporal perspective, these sources were therefore not deemed suitable, for example; when did the area highlighted as at risk actually flood, if at all?

The most reliable flood evidence that could be used as a source of ground truth data was drone footage published on YouTube of the December 2019 floods in Sussex. Footage was found of flooding on the Ouse at Great Walstead, approximately 2km away from the NFM features at Woodsland Farm. This depicted flood extent on 22nd December (two days after the peak flood) that could be digitised in QGIS using a Google Map base layer. The footage was also used to digitise areas that could reasonably be assumed would not be breached, on the basis of their relative distance from the flood and that showed no obvious evidence within them of receded flood. There is an accepted risk though that these areas could have been inundated after the footage was taken.

Two other sources of ground truth were considered suitable; photographs found on Facebook of flooding at the Anchor Inn, situated at Barcombe, 18km downstream of the Woodsland Farm NFM features during the flood peak on 20th December. Again, from these records, flood extent could be digitised using Google Maps to create a polygon of known flood waters. From an on-site meeting held with the SFI, specific areas of persistent flood and reliable ‘dry’ areas were recorded. These samples were small, ranging from 0.5 to 1.2 hectares, but provided certainty of flood and dry locations at the flood peak on the Cockhaise Brook itself.

Table 2.7.1: *Temporal and locational variances for the selected ground truth sample sites.*

Ground Truth Sample Location	Euclidean Distance From SFI Site (km)	River	Area (Ha)	River Gauging Station	Flood Record Sample Date	Flood Peak Date	Variance to Flood Peak (Days)
NFM features, Woodsland Farm	0	Cockhaise Brook, Ouse	1.4	Freshfield Bridge	Known Site	20/12/19	0
Anchor Inn, Barcombe	13	Ouse	1.2	Anchor Gates	20/12/19	20/12/19	0
Great Walstead	2	Scrase Stream, Ouse	9.7	Freshfield Bridge	22/12/19	20/12/19	2
Alfriston	28	Cuckmere	33.3	Sherman Bridge	22/12/19	20/12/19	2
Hellingly	26	Bull	18.4	Leabridge	27/12/19	20/12/19	7
Mock Bridge, Henfield	19	Adur	79.8	Sakeham Weir	22/12/19	20/12/19	2
Wineham	15	Adur	80.7	Sakeham Weir	20/12/19	20/12/19	0

Totaling 11 hectares, the Ouse sample sites did not provide enough coverage upon which to base an accuracy assessment of the proposed flood mapping technique. Extensive drone footage of the Sussex floods was found on the nearby rivers Bull, Cuckmere and Adur, ranging from 20th to 27th December. Further sample areas were digitised based on this footage, ranging in area from 1 to 35 hectares. This required the subset of the S-1 image to be extended across the three river catchments. In total, an array of 22 suitable ground truth samples were used from 6 different sites. Table 2.7.1 above sets out the temporal and locational issues to be considered in using these samples. The largest temporal difference of 7 days is at Hellingly. The Euclidean distance from the NFM features provides context as to the variable distance of each sample from the AOI.

2.8. Ground Truth Datasets

Ground truth analysis was conducted on the consecutive days of 20th and 21st December 2019 to capitalise on available S-1 passes for these dates, to capture the backscatter effects of different wind conditions. S-1A descending imagery on 20th December corresponds with baseline data on 9th November 2019 in terms of the same satellite pass and at a time when the river was at a seasonally consistent low. Descending S-1B imagery was used for 21st December. The baseline date of 20th November 2019 again corresponds with the same satellite pass and low river levels.

Table 2.8.1: *Ground truth S-1 imagery in relation to wind conditions (as recorded at Shoreham-on-Sea weather station).*

S-1 dataset	Date	Wind Speed (km/h) & Direction	Date	Wind Speed (km/h)
Flood Image	20/12/19	17.3 (SE)	21/12/19	29.2 (S)
Reference Image	09/11/19	15.1 (SW)	20/11/19	24.1 (NE)

Table 2.8.1 above shows the compatibility of the flood and reference dates for the S-1 datasets used in relation to wind conditions. This takes into account possible variations in backscatter intensity value due to wind that will have a more adverse effect on VV polarised data.

2.9. Optimum Threshold Coefficient Parameters

To ensure that the optimum threshold parameters were applied to the AOI, a range of threshold values were classified in the flood/dry difference image for the ground truth samples. Based on the CDAT criterion devised by Long et al, coefficients ranging from 1 to 1.5 for flood waters and 2 to 2.5 for inundated vegetation were used to calculate histogram threshold values (2014).

From the results of the accuracy assessment, the optimum threshold values were applied to detect flood waters and inundated vegetation in the NFM AOI.

2.10. Evaluation of NFM Features in Relation to the Difference in Flood Characteristics Post Installation

An evaluation of the NFM features on Cockhaise Brook was undertaken on the basis of how comparable flood events before and after installation of flood management measures changed in terms of spatial characteristics. To aid this evaluation, Cockhaise Brook was broken down into identified functional zones as shown in Figure 2.10.1 below, based on the following:

- Zone 1 – area immediately to the north of the bridge on Keysford Lane, where whilst visiting the project, the author's own observations identified evidence of recent flood waters breaching the lane. There is also a small stream in this location, which may be affected by the installation during high flows. Analysis of the pre- and post-restoration flood events would identify potential changes in extent to this area, indicating any possible adverse effects upstream of the NFM installation.
- Zone 2 – area immediately upstream of the main NFM scrape features. Smaller scale floodplain reconnections have been carried out in this area, as well as Black Poplar tree planting to improve soil drainage. Again, analysis of change to this area would highlight

how the NFM measures may have affected flood extent immediately upstream and provide insight into any possible effects of the smaller scale NFM measures.

- Zone 3 – the main NFM scrapes and their immediate area. Changes in flood attenuation due to the scrapes could be quantified to provide specific evidence as to the direct function the scrapes provide in allowing high river levels to flow into reconnected floodplain.
- Zone 4 – this zone was split down to take account of the effect of the Holywell weir. Overall, this zone was analysed for how flood area and form may have changed after the installation of the main scrapes immediately upstream.
    - Zone 4a – area immediately downstream of the main scrapes to the confluence with Danehill Brook, below which is the Holywell weir. The weir is a remnant of the brook's previous hydrologic function in providing power for the long defunct Cockhaise Mill. Changes in flood extent to this area would provide a measure as to how new attenuation volume created by the main scrapes, affects flood area and spatial form immediately downstream, up to the engineered break in flow created by the weir. There are also two more areas of planted Black Poplar, around which any change in flood extent or form could be analysed in more detail (realistically, these new wooded areas will take a long time to establish, but any detected changes would be relevant).
    - Zone 4b – this area is immediately downstream of Holywell weir. A smaller scrape has been formed here, along with more planting of Black Poplar trees.
- Zone 5 - The main tangible aim of the SFI project is to mitigate flood inundation around the Cockhaise Mill site. The topography in the vicinity of the mill defines a larger potential area of flood inundation on the southern side of the main road dissecting the zone. This includes an area where the SFI project has reconnected the floodplain to Cockhaise Brook. Changes in flood area and form in this location will provide an indication as to how successful the upstream NFM features have been in mitigating and diverting flood waters away from the mill site.
- Zone 6 – This is the stretch of Cockhaise Brook immediately to the north of the confluence with the main Sussex Ouse. Analysis would seek to identify how flood characteristics may have changed at this point.

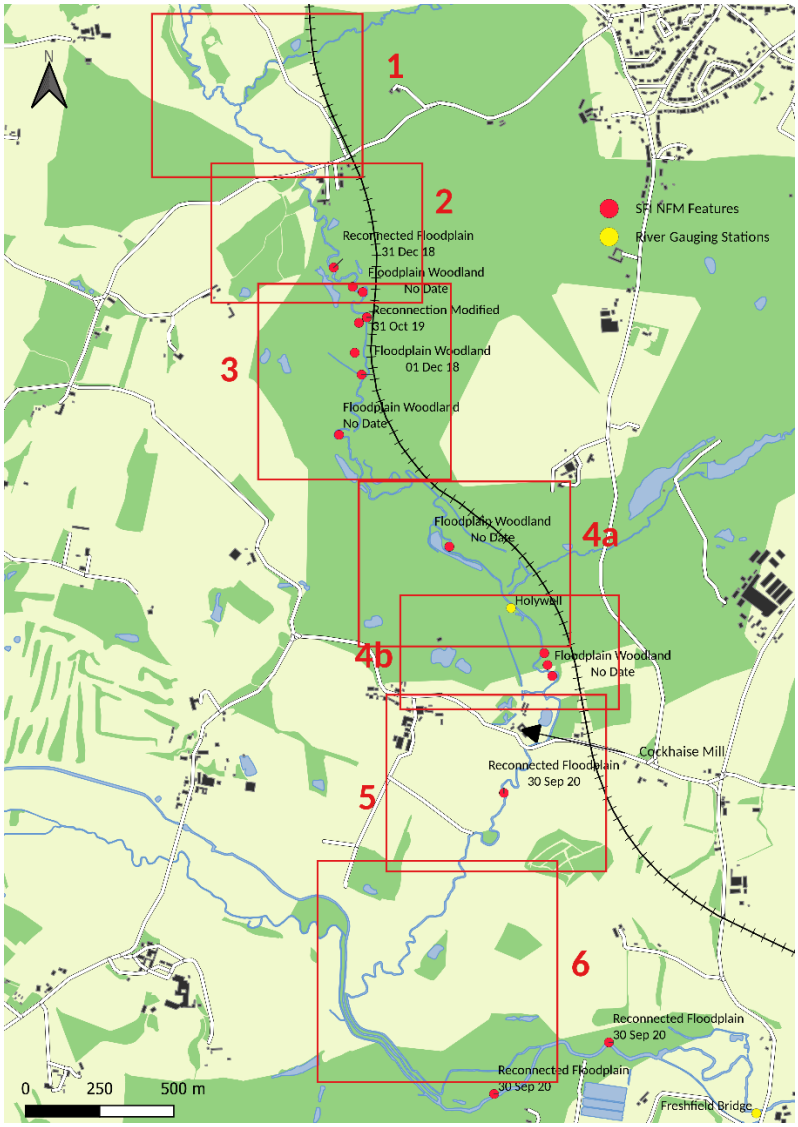

Figure 2.10.1: *Map of the identified functional zones of Cockhaise Brook.*

A zonal perspective provides a framework to ascertain changes in flood extent in relation to how the main NFM features have been designed to function and to interpret any spatial effects that may be identified. Analysis was also conducted on the same basis in aggregate for all of the NFM measures employed on Cockhaise Brook. Zone boundaries were defined to the east by the rail line embankment running most of the length of the brook and to the west by hilly terrain. Therefore, only flood waters located between the brook and these features were considered as having any potential causal relationship with the NFM features.

Fluvial flood water dispersal in relation to Cockhaise Brook was analysed by constructing buffer rings around the brook, from which a GIS intersection operation delineated inundation area in each buffer zone. Patterns of dispersal area in relation to distance from the brook were compared pre- and post-NFM to identify if NFM measures may have influenced the restriction of flood water extent away from the source. This is specific to Cockhaise Brook, as it is bounded for much of its length by the railway embankment and steep terrain. For longer sections of the Sussex Ouse, where there are more changes in form of the river, more nuanced assessments of the relationship of flood waters to their origin could not be answered with this type of analysis. However, this provided a relevant relative indication of dispersal of pre- and post-NFM flood events in this situation. Considering the

modest size of Cockhaise Brook, a multi-ring 20m buffer was considered to provide reasonable incremental zones of dispersal up to 400m from the flood source.

Buffer analysis was also used to identify where post-NFM flood waters have concentrated around NFM features on Cockhaise Brook and if these concentrations differ from the pre-NFM flood form. 50m buffers were constructed around each NFM feature to calculate flood waters detected in this area.

Another indicator used to assess the dispersal of flooding at a zonal scale was the perimeter length of a constructed convex hull around inundation extent. A convex hull provides a measure of compactness of flood extent. Again, this is project-specific, where compactness is considered desirable.

2.11. NFM Evaluation Summary

As has been demonstrated in the development of this methodology, to evaluate how NFM measures have changed the flood characteristics of Cockhaise Brook, comparable data pre and post NFM installation for a substantial flood event was not possible. S-1 data availability and the relatively short window between the advent of S-1 imagery and the NFM installation required that the comparison was based on the flood at its peak post-NFM, but in its ascendance/descendance for the pre-NFM event. Owing to this issue, it was considered most beneficial that the evaluation assess the two stages of the pre-NFM extent in aggregate and separately. This therefore took into account the question of whether simply aggregating the extents may not actually depict the true extent of the flood at its peak. Also, simply comparing flood area is misleading in terms of this comparability issue and in the fact that the essence of the NFM design is to naturally manage, not reduce flood extent.

Therefore, a scorecard formulated as below was used to summarise the evaluation on a greater zonal basis that directly takes account of the NFM features and individual zones.

Using these classifications, the scorecard compared pre- and post-NFM scenarios as follows:

- Increase/similar/decrease in detected flood area
- Visual assessment of change/no change in form of flood extent using maps of detected flood. This is a subjective assessment of the flood in relation to:
    - dispersal from the brook
    - key geographic features such as residential properties or roads
    - NFM features in close proximity.
- Increase/similar/decrease in compactness of zonal flood extent. This was assessed by creating a convex hull covering the minimum area of the full extent of flood waters in each zone. The perimeter length of each polygon was compared for both flood events to measure any change in overall flood extent.

Context was applied to these classifications as, for example an increase in flood waters where attenuation has been designed in the NFM installation is positive, whereas increases in flood water in a zone containing residential properties could be construed as a negative outcome. Also, where change did not occur, this could attract any of the positive, negative or neutral outcome classifications, due to the assimilate comparability issue of the pre-NFM ascendant/descendant stages with the post-NFM peak or because of design intentions.

3. Results

3.1. Optimum Pre-Processing Parameters

The Lee and Gamma MAP filters were tested during the ground truth flood detection operation. Results showed no difference in flood detection in either the dry or flood ground truth areas between these filters. Therefore, it was deduced that no improvement in flood detection, nor introduction of error from false detection in dry areas was evident in using the Gamma MAP filter in comparison with other suitable speckle filters.

3.2. Ground Truth Flood Detection Results

The geographic coverage of the ground truth sites is illustrated below in Figure 3.2.1, together with the nearest gauging station used to temporally assess flood peak.

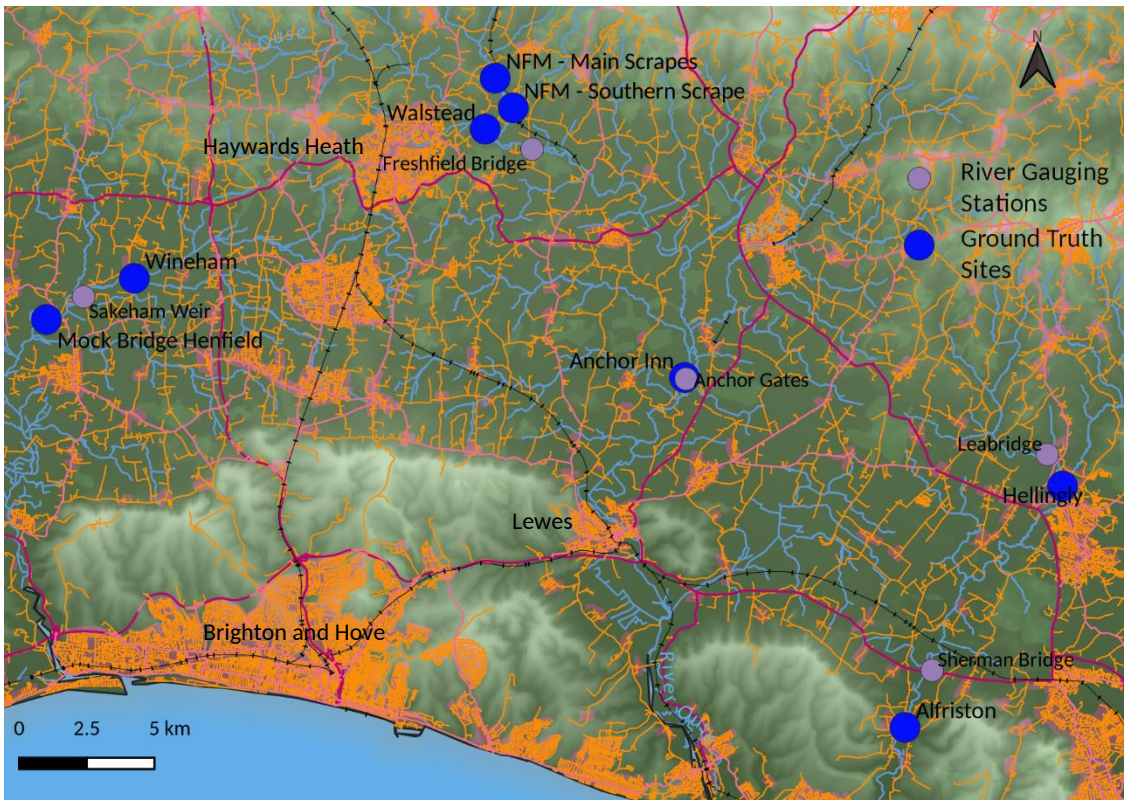

Figure 3.2.1: *Map of the ground truth site locations and nearest river gauging station.*

Table 3.2.1: *Flood waters and inundated vegetation detection in ground truth areas for the 20th December 2019 flood event.*

Ground Truth Sample	Weather Conditions	Calm		Windy	
	Overall Area Ha	20th Dec 2019 vs 9th Nov 2019 VH	20th Dec 2019 vs 9th Nov 2019 VV	21st Dec 2019 vs 20th Nov 2019 VH	21st Dec 2019 vs 20th Nov 2019 VV
		% Flood/Inundated Vegetation Detection			
Dry Ground Truth Total	122.57	5.6	9.8	9.5	13.3
Flood Ground Truth Total	101.84	53.0	53.4	56.5	55.6

Table 3.2.1 above sets out the proportion of ground truth polygons where open flood waters and inundated vegetation have been detected for the 20th December 2019 flood event in Sussex. Intersection analysis results for CDAT operations undertaken with 20th December and 21st December flood imagery and their respective baseline dates, are shown for known dry and flooded areas. These results are based on the optimum histogram thresholds determined from the conclusion of the accuracy assessment below. No attempt has been made to remove very small areas with GIS operations, such as a minimum size sieving process, due to the relatively small AOI in which flood patterns were intended to be evaluated on Cockhaise Brook. The rate of false positives in known dry areas during the flood is generally low (between 5.6 and 13.3%). Flood detection rates in areas of know inundation vary slightly between 53 and 56.5%.

Table 3.2.2: *Mean backscatter values for lakes within the Ground Truth AOI in dry and flood scenarios.*

Scenario	Image Date	Polarisation	Sample Feature	Mean Sigma θ DB	Difference Sigma θ DB
Dry	9th Nov 2019	VH	Lakes	-17.65	2.50
Flood	20th Dec 2019	VH	Lakes	-15.15	
Dry	20th Nov 2019	VH	Lakes	-16.74	0.86
Flood	21st Dec 2019	VH	Lakes	-15.88	
Dry	9th Nov 2019	VV	Lakes	-11.50	2.06
Flood	20th Dec 2019	VV	Lakes	-9.44	
Dry	20th Nov 2019	VV	Lakes	-10.64	0.11
Flood	21st Dec 2019	VV	Lakes	-10.53	

Using a lake polygon layer for water bodies within Sussex, the zonal statistics of backscatter values in these regions for each S-1 image raster layer were calculated. The overall mean average of water body backscatter values was then established as included in Table 3.2.2. Despite different wind conditions, both VV and VH polarisation radar responses did not differ enough to meet the thresholds used to determine open flood water or inundated vegetation.

Figure 3.2.2 below shows a scatter graph of detected change for sites representing dry conditions on 20th December 2019 (the peak of the flood on the Sussex Ouse), against the reference date of 9th November 2019. The horizontal axis plots the percentage of flood water detected, which as these sites have been selected as being certain of no flooding would theoretically be low. The vertical axis

shows the variance from the peak flood on that particular river on 20th December, when the flood satellite image was sensed. The colour of each point represents the area in which the site is situated. Polarisation has been symbolised as circles for VH and triangles for VV. For this event, the variance from the peak on 20th December was not large, as generally all of the rivers upon which the sites are located were at a very high flow level. Points are therefore spread according to the proportion of flood water detected at each dry site across the bottom of the vertical axis. The most significant observations are the relatively large proportion of flood water/inundation in VV polarisation for Alfriston (28%) and Hellingly (20%) in what are areas known not to have been breached.

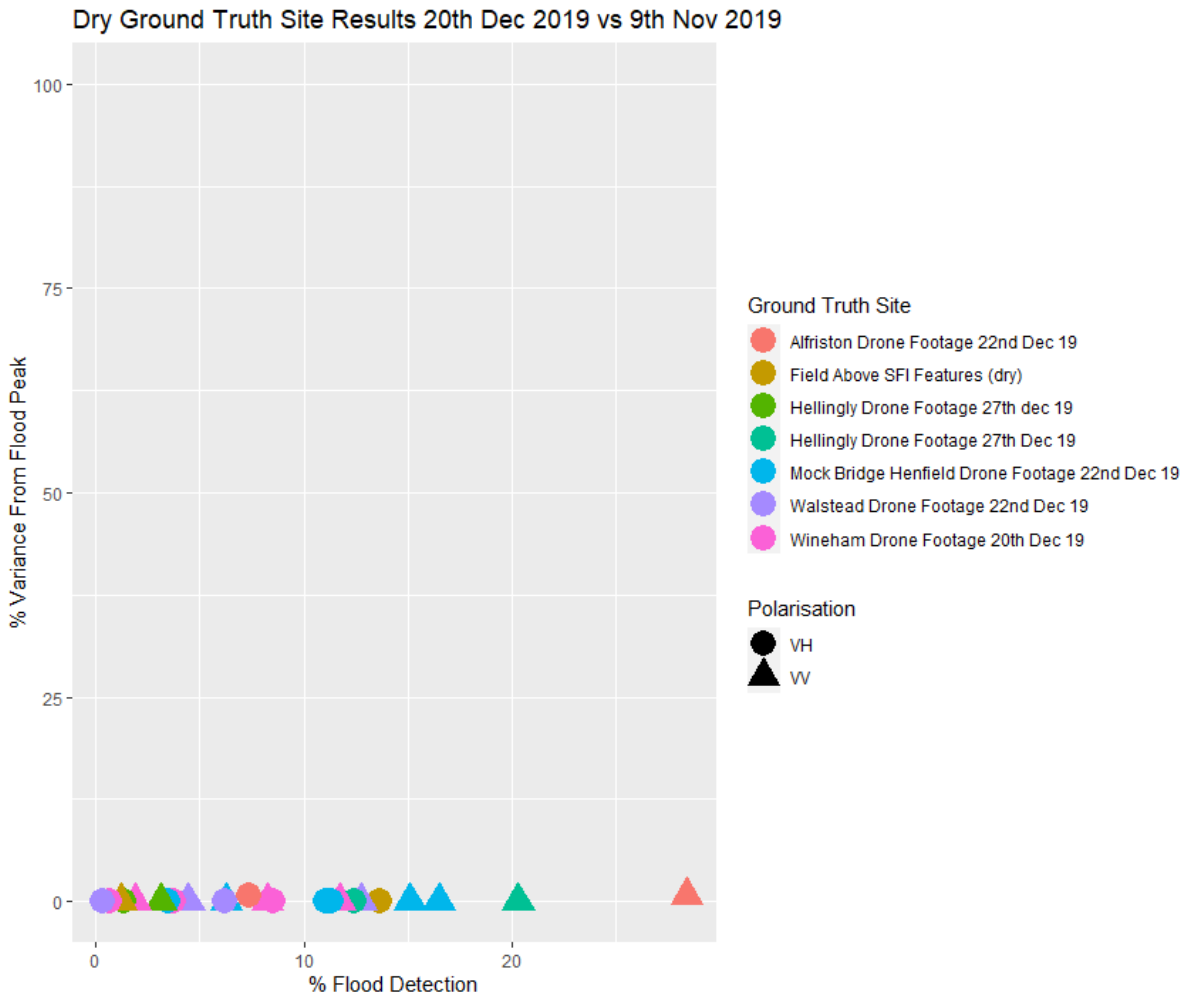

Figure 3.2.2: *Scatter graph of river level variance the image date of 20th December 2019 to the local flood peak and of flood waters detected in ground truth sites representing dry conditions in a flood.*

Also, representing known dry sites on 21st December 2019 against the baseline date of 20th November 2019, the scatter graph in Figure 3.2.3 below shows on the vertical axis that there is much more variance from the local flood peak. There are also large proportions of flood waters detected in these dry sample sites; 25% and 23% in VV and VH polarisation respectively for Mock Bridge and 20% in VV for Wineham.

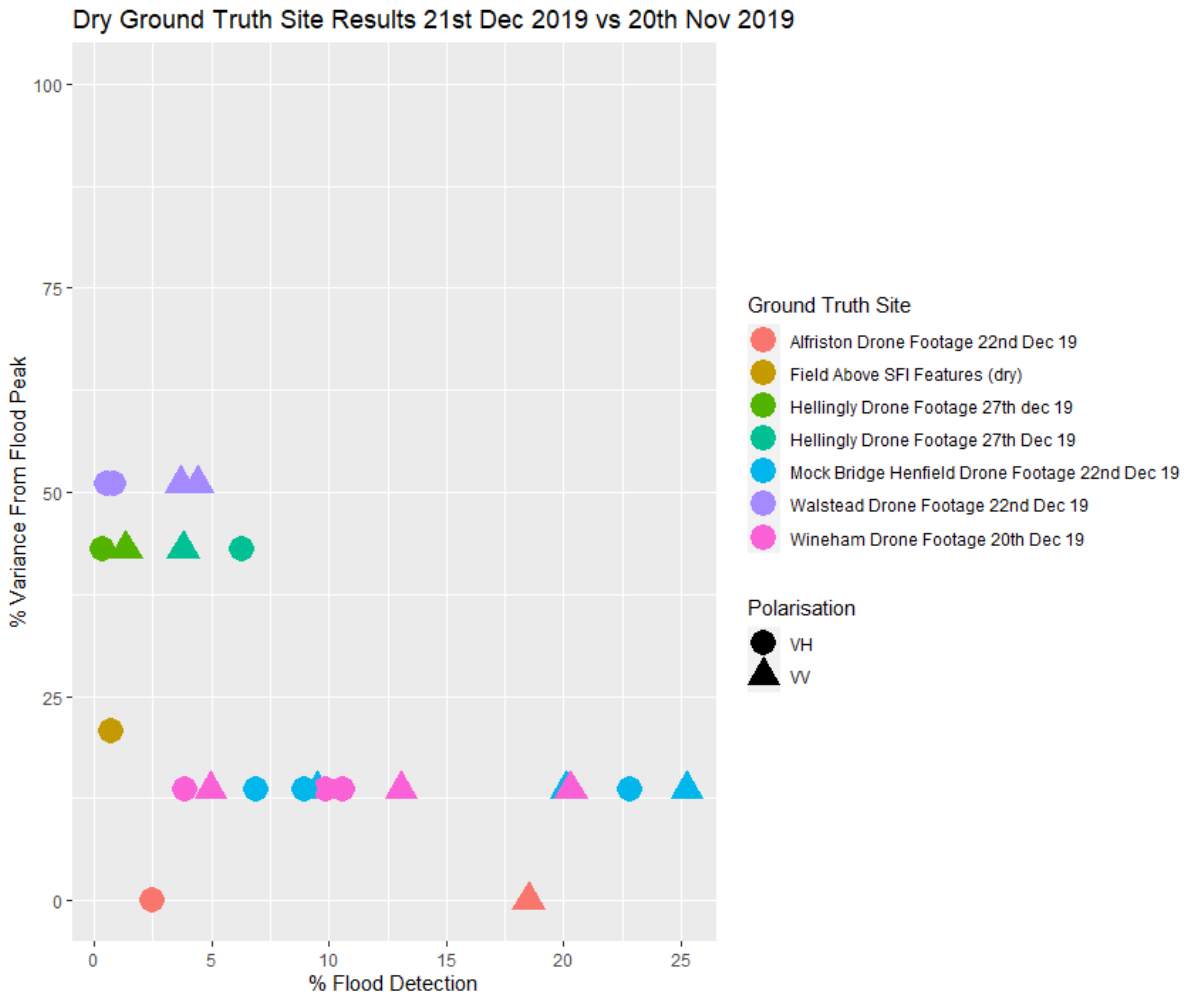

Figure 3.2.3: *Scatter graph of river level variance on the image date of 21st December to the local flood peak and of flood waters detected in ground truth sites representing dry conditions in a flood.*

The scatter graphs of ground truth sites with certainty of flood coverage are shown in Figures 3.2.4 and 3.2.5 below for 20th December and 21st December respectively. For the 20th December S-1 image, Alfriston apart (both polarisations), there is a concentrated grouping of results between 42 and 96%. The spread of results in Figure 3.2.5 for 21st December is far greater. Even without Hellingly (both polarisations) and the very small site of the NFM features, the range is from 10 to 82%.

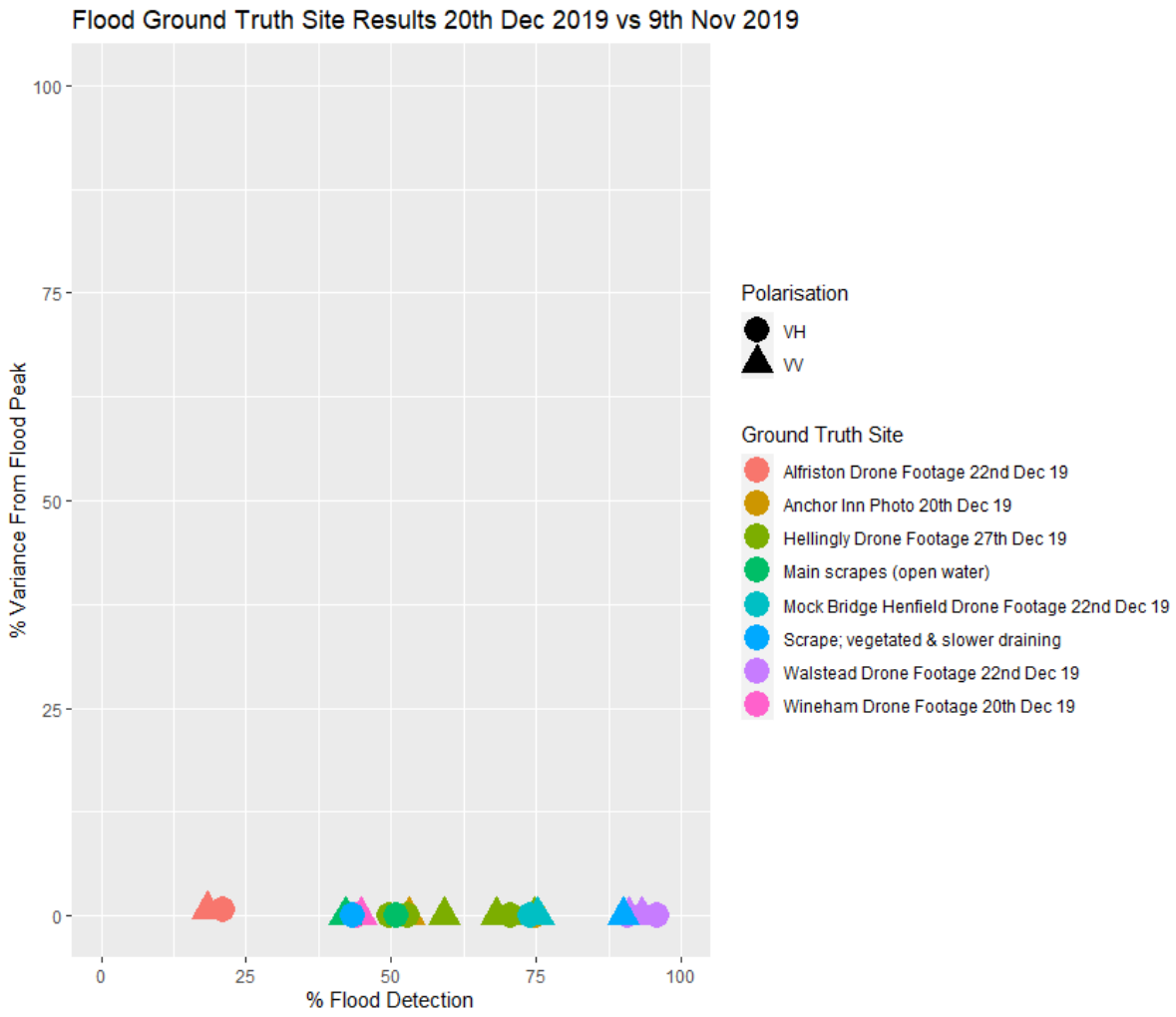

Figure 3.2.4: *Scatter graph of river level variance on the image date of 20th December 2019 and of flood waters detected in ground truth sites representing certain areas of flood.*

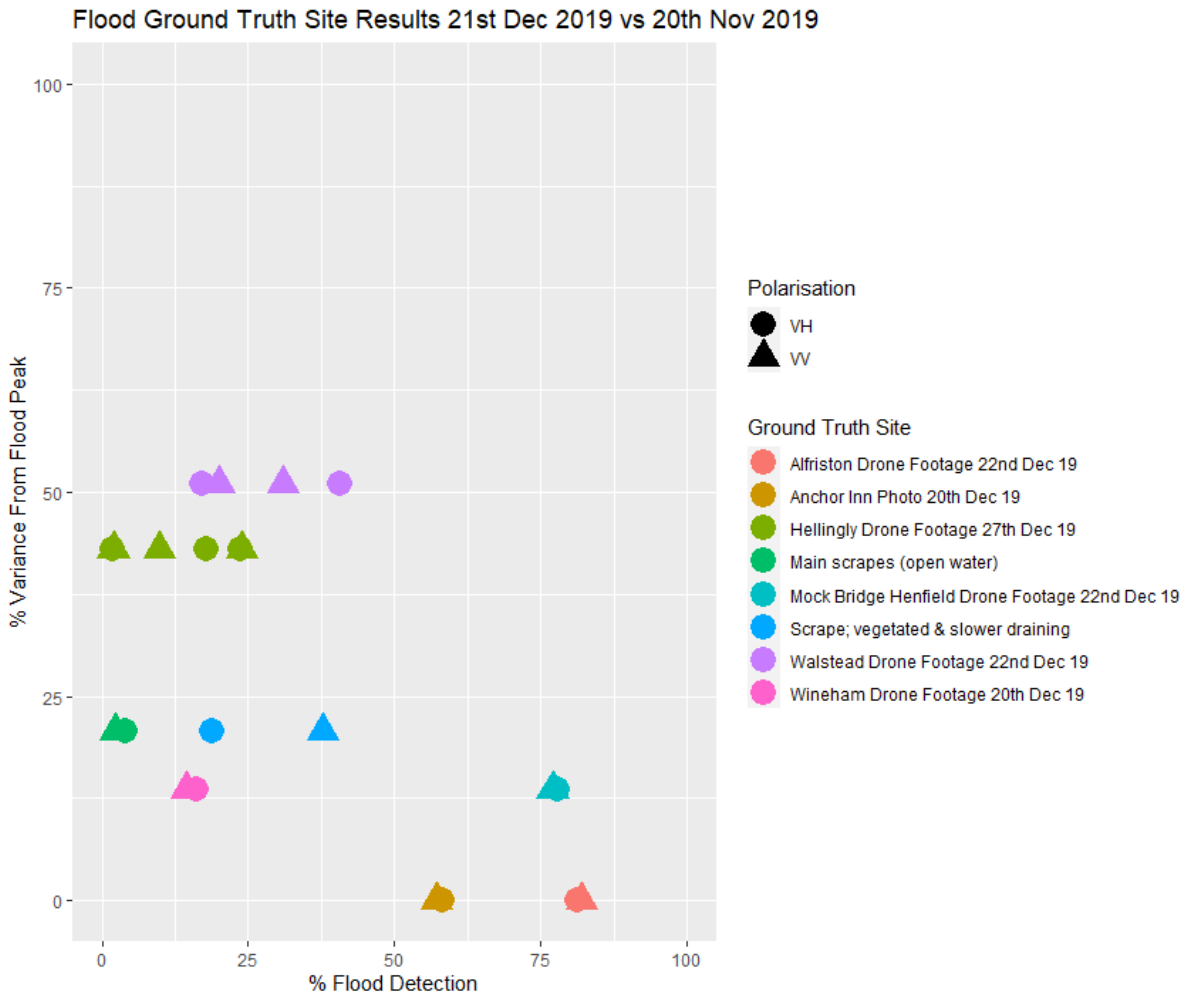

Figure 3.2.5: *Scatter graph of river level variance on the image date of 21st December 2019 and of flood waters detected in ground truth sites representing certain areas of flood.*

3.3. Ground Truth Flood Detection Accuracy Assessment

A range of coefficient values were used to produce a multiple classification of backscatter change between the flood and 'dry' S-1 images to detect flood waters on 20th and 21st December 2019. For open flood waters, coefficient values between 1 and 1.5 were classified (Long et al deduced 1.5 to be the optimum value (2014)). A range between 2 and 2.5 was used for inundated vegetation (Long et al deduced 2.5 to be the optimum value (2014)). The area of detected flood waters and inundated vegetation contained within the ground truth sites across Sussex was then calculated, from which confusion matrices were produced to assess accuracy. As inundated vegetation instances were very low, they have been combined with the flood waters into an overall flood area total.

Table 3.3.1: *Confusion matrix for the optimum CDAT coefficient values in VH polarisation in windy conditions for the flood image date of 21st December and reference image of 20th November 2019 for the ground truth sites.*

Polarisation:	**VH**			
Long Coefficient;				
Flood water	**2.5**			
Flooded Vegetation	**1.3**			
Flood Image Date:	**21/12/2019**			
Reference Image Date:	**20/11/2019**			
	Digitised references			
S-1B 6am	**No Flood Ha**	**Flood Ha**	**S-1 Total Ha**	**User's %**
No Flood Ha	111.0	44.3	155.3	71.5%
Flood Ha	11.6	57.6	69.2	83.2%
Reference Total Ha	122.6	101.9	224.5	
Producer's %	90.5%	56.5%		
			Total Accuracy =	75.1%
			Kappa Statistic =	0.484

Table 3.3.1 above presents the optimum results of the intersection of flood water and inundated vegetation in dry and flood ground truth sites in VH polarisation for the windy conditions of 21st December 2019 (29km/h). Reducing the coefficient for inundated vegetation had the effect of increasing false positives, without any beneficial increase in correctly detected areas. The optimum setting of 2.5 therefore concurs with that used by Long et al (2014). Whilst the reduction in the flood water coefficient to 1.3 resulted in more false positives, there was an overall increase in accuracy due to greater detection of correct flood waters. A coefficient of 1.2 achieved the same Kappa statistic, but a slightly lower total accuracy of 75%, due to a greater proportion of false positives in relation to the additional flood waters/inundated vegetation detected.

83% of the total area of flood/inundated vegetation detected could be correctly verified by intersecting with certain records of flood in the ground truth sites. Therefore, 17% of detected flooding intersected with certain records of dry ground in the ground truth sites. 57% of known flooded areas in ground truth sites were correctly detected using CDAT and 91% of known dry areas were correctly classified as such. Overall, the total accuracy of the CDAT technique with optimum coefficients employed was 75% in VH polarisation. The Kappa statistic is 0.484, which can be interpreted as a 48% better method of flood detection than one resulting from chance.

Table 3.3.2: *Confusion matrix for the optimum CDAT coefficient values in windy conditions in VV polarisation for the flood image date of 21st December and reference image of 20th November 2019 for the ground truth sites.*

Polarisation:	**VV**			
Long Coefficient;				
Flood water	**2.5**			
Flooded Vegetation	**1.2**			
Flood Image Date:	**21/12/2019**			
Reference Image Date:	**20/11/2019**			
	Digitised references			
S-1B 6am	**No Flood Ha**	**Flood Ha**	**S-1 Total Ha**	**User's %**
No Flood Ha	106.4	45.2	151.6	70.2%
Flood Ha	16.2	56.7	72.8	77.8%
Reference Total Ha	122.6	101.9	224.4	
Producer's %	86.8%	55.7%		
			Total Accuracy =	72.7%
			Kappa Statistic =	0.435

Table 3.3.2 above presents the optimum results in VV polarisation. Again, the optimum setting of 2.5 concurs with Long et al (2014) for inundated vegetation. This time, the open flood water coefficient was reduced to 1.2, as this produced a slightly better Kappa statistic than the 1.3 setting settled on in the VH accuracy assessment.

78% of the total area of flood/inundated vegetation detected could be verified by intersecting with certain records of flood in the ground truth sites. Therefore, 22% of detected flood intersected with certain records of dry ground in the ground truth sites. 56% of known flooded areas in ground truth sites were correctly detected using CDAT and 87% of known dry areas were correctly classified as such. Overall, the total accuracy of the flood detection technique employed was 73% in VV polarisation. For windy conditions, the Kappa statistic is 0.435, lower than the results in VH.

Table 3.3.3: *Confusion matrix for the optimum CDAT coefficient values in VH polarisation in calmer conditions for the flood image date of 20th December and reference image of 9th November 2019 for the ground truth sites.*

Polarisation:	**VH**			
Long Coefficient;				
Flood water	**2.5**			
Flooded Vegetation	**1.2**			
Flood Image Date:	**20/12/2019**			
Reference Image Date:	**09/11/2019**			
	Digitised references			
S-1A 6am	**No Flood Ha**	**Flood Ha**	**S-1 Total Ha**	**User's %**
No Flood Ha	115.8	48.9	155.2	70.3%
Flood Ha	6.8	53.0	69.2	88.7%
Reference Total Ha	122.6	101.9	224.4	
Producer's %	94.5%	52.0%		
			Total Accuracy =	75.2%
			Kappa Statistic =	0.482

Table 3.3.3 above presents the optimum results of the intersection of flood water and inundated vegetation in dry and flood ground truth sites in VH polarisation for 20th December 2019, where weather conditions were less windy (17.3km/h). The flood water coefficient was reduced to 1.2, as this produced a better Kappa statistic and total accuracy than the 1.3 setting used in the VH polarisation in the windier conditions of 21st December 2019.

A greater total area of flood/inundated vegetation was detected (89%) that could be verified by intersecting with certain records of flood in the ground truth sites. Therefore, 11% of detected flood intersected with certain records of dry ground in the ground truth sites. However, the percentage of known flooded areas in ground truth sites correctly detected using CDAT was lower at 52%. 95% of known dry areas were correctly classified as such using CDAT. Overall, the total accuracy of the flood detection technique employed was 75% in VH polarisation, almost the same as in windy conditions on 21st December. The Kappa statistic of 0.482 is slightly lower.

Table 3.3.4: *Confusion matrix for the optimum CDAT coefficient values in VV polarisation in calmer conditions for the flood image date of 20th December and reference image of 9th November 2019 for the ground truth sites.*

Polarisation:	**VV**			
Long Coefficient;				
Flood water	**2.5**			
Flooded Vegetation	**1.0**			
Flood Image Date:	**20/12/2019**			
Reference Image Date:	**09/11/2019**			
	Digitised references			
S-1A 6am	**No Flood Ha**	**Flood Ha**	**S-1 Total Ha**	**User's %**
No Flood Ha	110.4	48.4	158.9	69.5%
Flood Ha	12.1	53.4	65.6	81.5%
Reference Total Ha	122.5	101.8	224.5	
Producer's %	90.1%	52.5%		
			Total Accuracy =	73.0%
			Kappa Statistic =	0.439

Table 3.3.4 above presents the optimum results in VV polarisation during calmer conditions. This time, the flood water coefficient was reduced to the lowest classified setting of 1.0, as correctly verified flood detection area was still greater than the increase in false positives.

At 82%, the total area of flood/inundated vegetation detected that could be verified by intersecting with certain records of flood in the ground truth sites was a better proportion than in windy conditions on 21st December. Therefore, 18% of detected flood intersected with certain records of dry ground in the ground truth sites. However, there was a lower proportion of known flooded areas in ground truth sites that were correctly detected using CDAT compared with more windy conditions (53% compared with 56%). At 90%, the proportion of known dry areas that were correctly classified as such using CDAT, performed better than in windy conditions. Overall, the total accuracy of the flood detection technique employed was 73% in VV polarisation, a 0.3% improvement compared with windy conditions. The Kappa statistic improved slightly by 0.004 to 0.439. In comparison with the VV results in more windy conditions, accuracy is marginally better.

3.4. Optimum Histogram Threshold Settings

Based on the accuracy assessments carried out in each polarisation and for the two image dates to account for different wind conditions, the optimum coefficient values to set open flood water and inundated vegetation thresholds were deemed to be 1.3 and 2.5 respectively in VH polarisation. For calmer conditions an open water coefficient value of 1.2 in VH polarisation provided the best detection rates.

3.5. Evaluation of NFM Features Using Optimum Coefficient Settings

For application to the Cockhaise Brook study area, optimum coefficient settings were defined directly from the results of the accuracy assessment carried out on the ground truth sites across Sussex. The proposed post-NFM flood event date for analysis of 27th November 2019 was an extremely windy day (64km/h easterly direction). The maximum wind speed for the flood event

upon which the ground truth accuracy assessments were based was 29km/h in a southerly direction. As VH polarisation results were most stable in windy conditions and correlate with previous research in being less susceptible to the surface roughening caused (Manjusree et al., 2012), the optimum coefficient settings of 1.3 for open flood water and 2.5 for inundated vegetation in this polarisation on the windiest day (21st December 2019) were used for the NFM evaluation.

The two cohorts of data for the pre-NFM event used slightly differing coefficients to take account of wind conditions. For the higher winds experienced in the 10th January/5th December flood/reference cohort, coefficient values as the post-NFM were used. For the 13th January/26th November flood/reference cohort, which were in calmer conditions, the lower coefficient value of 1.2 was used to reflect the findings of the accuracy assessment.

3.6. Flood Detection Results on Cockhaise Brook

Table 3.6.1: *Detected areas of open flood water/inundated vegetation in each functional zone of Cockhaise Brook.*

Functional Zone	Detected Flood Area Ha		
	Pre-NFM Flood Event		Post-NFM Flood Event
	10th Jan 2016 vs 5th Dec 2015	**13th Jan 2016 vs 26th Nov 2015**	**27th Nov 2019 vs 9th Nov 2019**
1 North of Keysford Lane	0.52	0.55	2.13
2 Above main scrapes	0.16	0.40	0.35
3 Main scrapes	0.14	0.24	0.56
4a Below main scrapes to Danehill Brook	0.24	0.86	0.90
4b Danehill Brook to above Cockhaise Mill	0.01	0.34	0.05
5 Cockhaise Mill to Freshfield	0.13	1.49	1.87
Greater NFM Zone (2-5)	0.68	3.33	3.73
6 Freshfield to Ouse	0.25	2.68	3.30
Total Cockhaise Brook	1.45	6.56	9.16

Total areas of flood detection by functional zone are shown above in Table 3.6.1. As flood image dates did not match the pre-NFM flood event peak, the area shown for 10th January should be viewed as the ascendancy of the flood and 13th January in its descending stage. Caution should therefore be used in comparing these totals with the post-NFM results.

GIS intersection analysis on the spatial extent of each flood event (the pre-NFM flood on 10th and 13th January and post-NFM on 27th November) was conducted to identify the full extent of where flooding occurred based on: only for one event; common pre-NFM flood areas; and areas corresponding with the post-NFM extent in one pre-NFM occurrence and both. Figure 3.6.1 below illustrates each scenario in all of the functional zones delineated. These are summarised as follows:

- Scenarios 1 -3 identify areas of flood detected only in the pre-NFM events.
- Scenarios 4-6 identify common areas of flood between one of both of the pre-NFM events and the post-NFM event.

- Scenario 7 identifies areas of flood detected only in the post-NFM event.

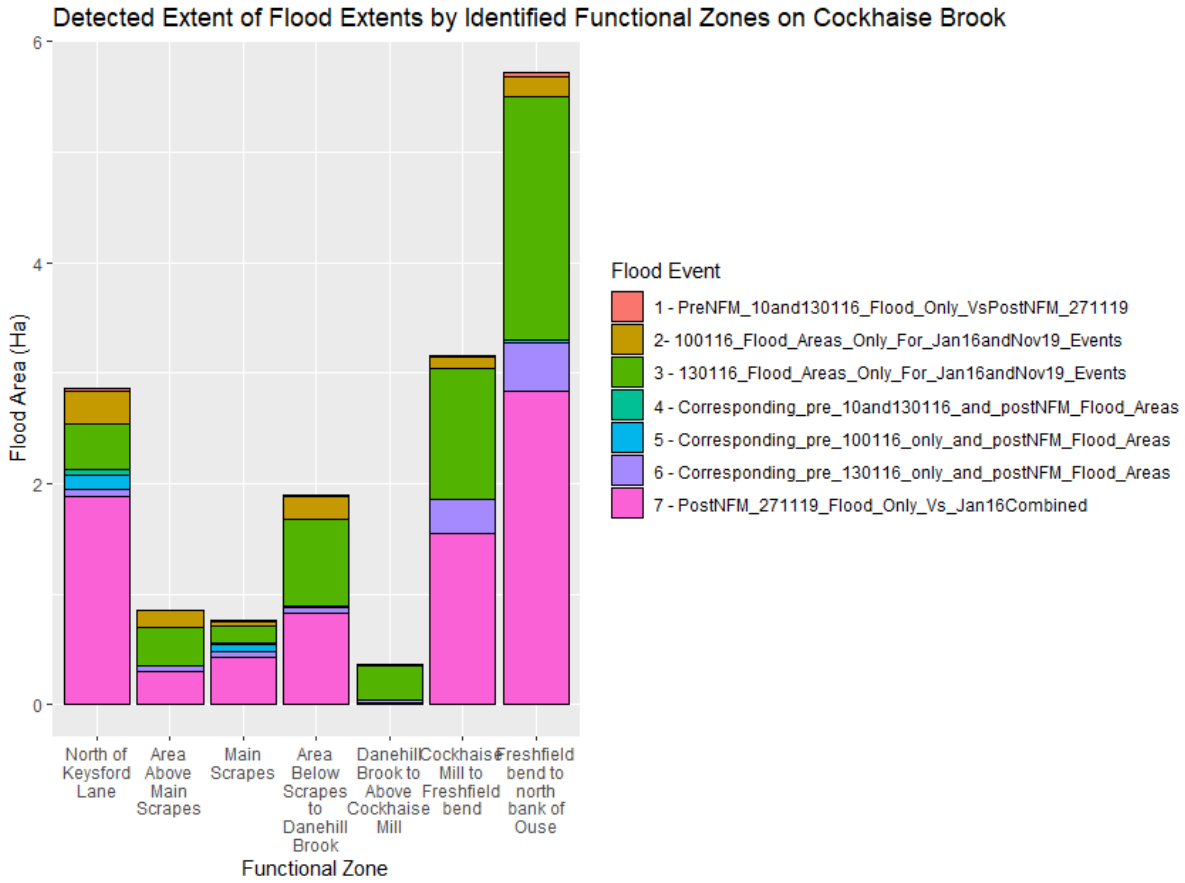

Figure 3.6.1: *Common and singular detected extent of pre-NFM and post-NFM flood events by functional zone.*

An overview map in Figure 3.6.2 below illustrates how Cockhaise Brook has been divided into the six identified functional zones.

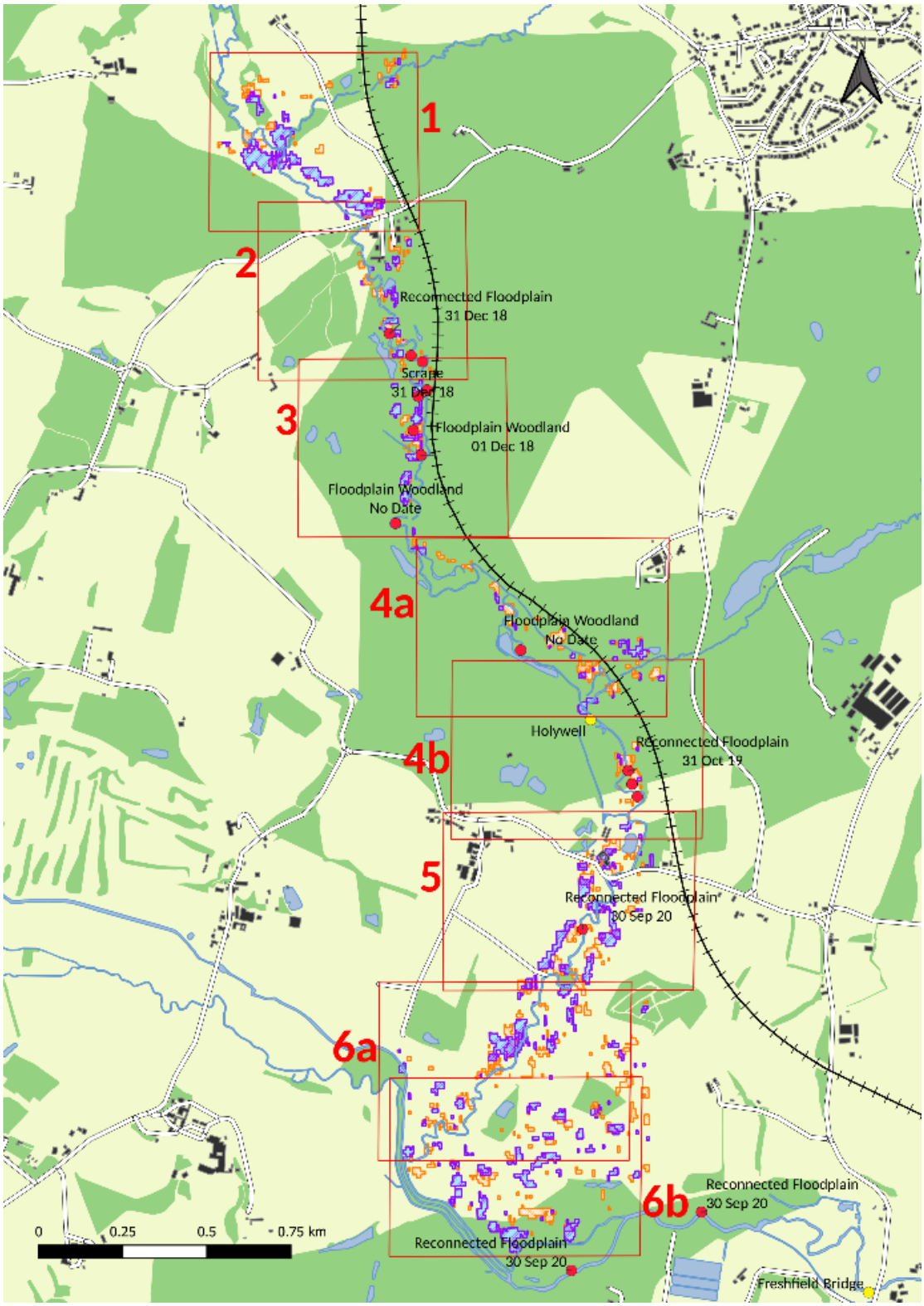

Figure 3.6.2: *Overview map of the identified functional zones on Cockhaise Brook.*

The legend in Figure 3.6.3 supports the interpretation of flood extent by pre- and post-NFM event and where NFM features are in relation to the inundated areas in the larger-scale zonal maps further on. These chart the extent of flood inundation across the functional zones in downstream order.

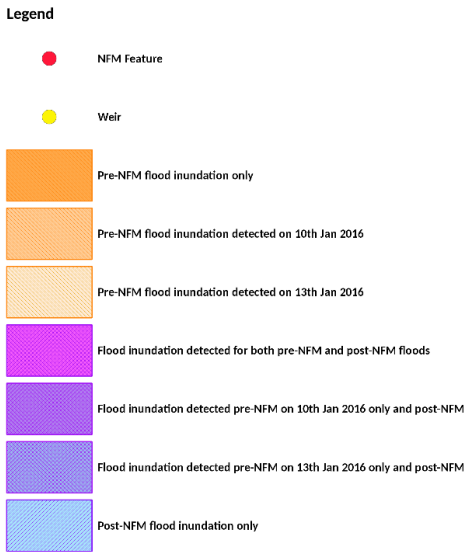

Figure 3.6.3: *Legend for detected flood areas in each event and NFM features in reference to the larger scale zonal maps.*

The map of Zone 1 north of Keysford Lane below in Figure 3.6.4 shows common areas of inundation for the pre- and post-NFM events where a stream flows into Cockhaise Brook and the brook flows under a road bridge to the downstream NFM installation. The substantially greater area of post-NFM flooding is generally either side of the bank between the confluence and the bridge.

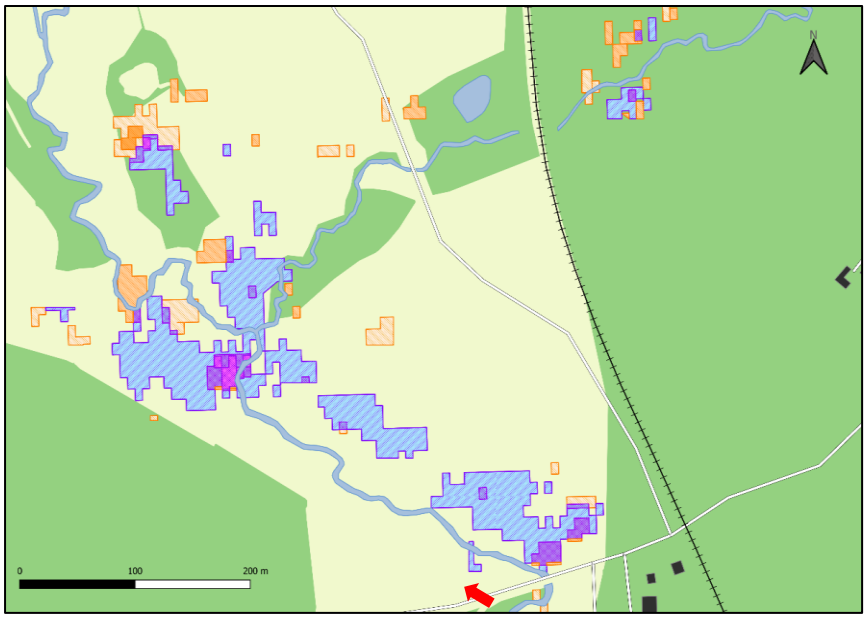

Figure 3.6.4: *Zone 1 – North of Keysford Lane - Map of flood inundation for pre- and post-NFM events (see key for flood references).*

Figure 3.6.5 below is a photograph of Zone 1 taken from the position of the red arrow shown on the map extract in Figure 3.6.4. This demonstrates why flood waters would be more concentrated on the western side of Cockhaise Brook, where there is steeper terrain running from the wooded area to the floodplain around the brook.

Figure 3.6.5: *The western bank of Cockhaise Brook on Zone 1 north of Keysford Lane.*

Zone 2 in Figure 3.6.6 below, displays very similar size areas of flood (0.40 ha pre-NFM and 0.35 ha post-NFM). However, there are very few common flood areas between the two events.

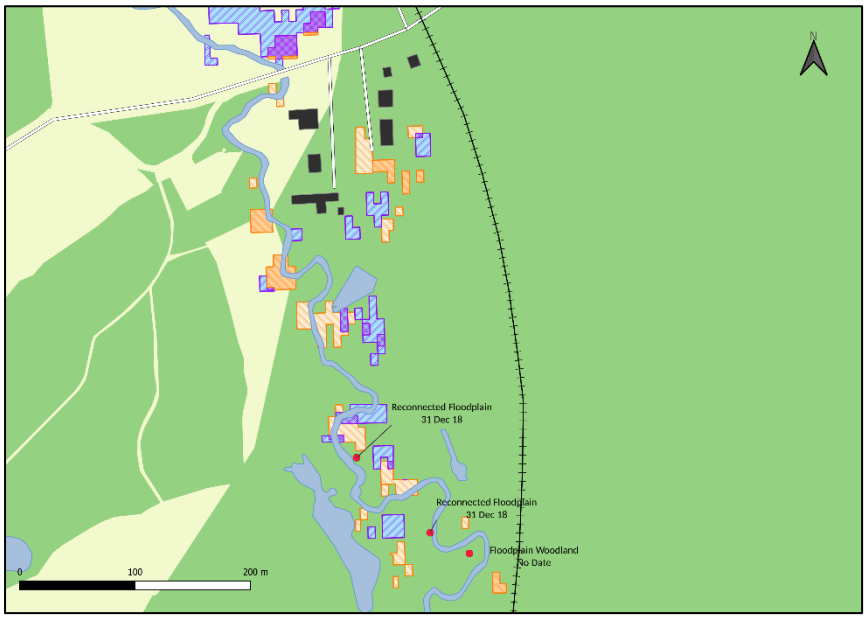

Figure 3.6.6: *Zone 2 – Area Above Main Scrapes - Map of flood inundation for pre- and post-NFM events (see key for flood references).*

Flood waters in Zone 3 have more than doubled in area from a maximum of 0.24ha pre-NFM to 0.56ha post-NFM. Figure 3.6.7 below shows the inundation accumulating around the installed scrapes, which have been designed to attenuate flood waters through an engineered cut in the raised bank to reconnect Cockhaise Brook with its original floodplain.

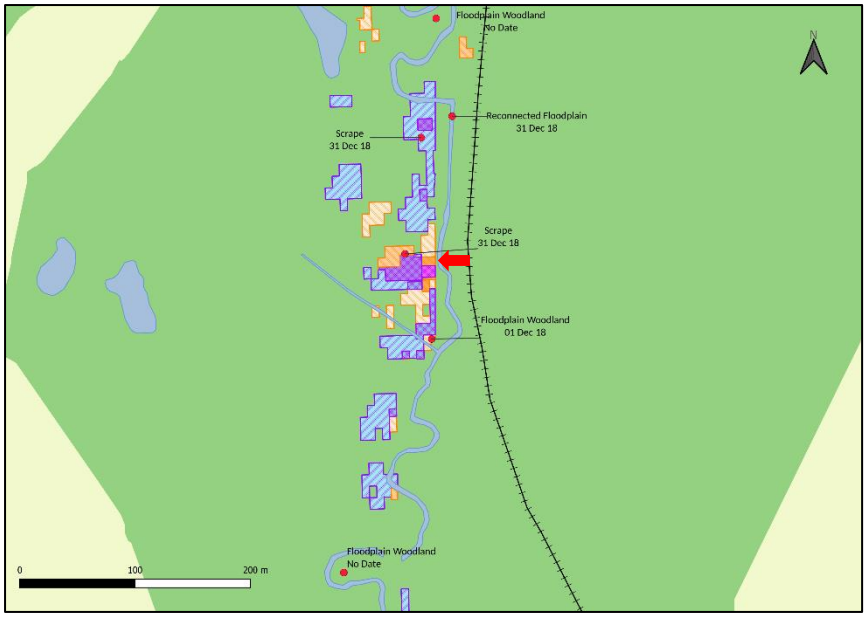

Figure 3.6.7: *Zone 3 – Main Scrapes - Map of flood inundation for pre- and post-NFM events (see key for flood references).*

Figure 3.6.8 below is a photograph of the secondary scrape in Zone 3, taken from the red arrow position shown on the map extract in Figure 3.6.7. The photo was taken during a particularly dry spell in mid-March, when the scrape was predominantly empty. It can be seen how Cockhaise Brook is bounded on its western side by higher ground.

Figure 3.6.8: *The secondary scrape in Zone 3 on Cockhaise Brook in a mainly dry state.*

The map of Zone 4a in Figure 3.6.9 below shows the confluence of Cockhaise Brook and Danehill Brook. The maximum pre-NFM flood area of 0.86ha is comparable to the 0.90ha of post-NFM flooding. However, again there is very little spatial consistency between the two events.

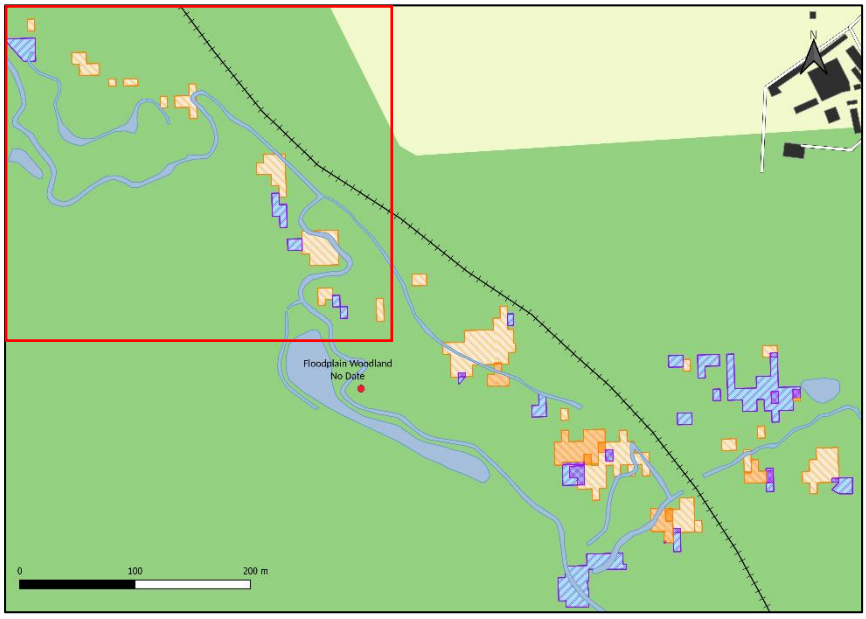

Figure 3.6.9: *Zone 4a – Area Below Scrapes to Danehill Brook - Map of flood inundation for pre- and post-NFM events (see key for flood references).*

Zone 4b, which in Figure 3.6.10 below is downstream of the Holywell weir in a south easterly direction, contains another smaller scrape feature and an area of floodplain tree planting. This map mostly depicts pre-NFM flood waters on 13th January. Very little area was detected in the ascendancy of the pre-NFM event (0.01 ha on 10th January) and for the post-NFM event (0.05ha).

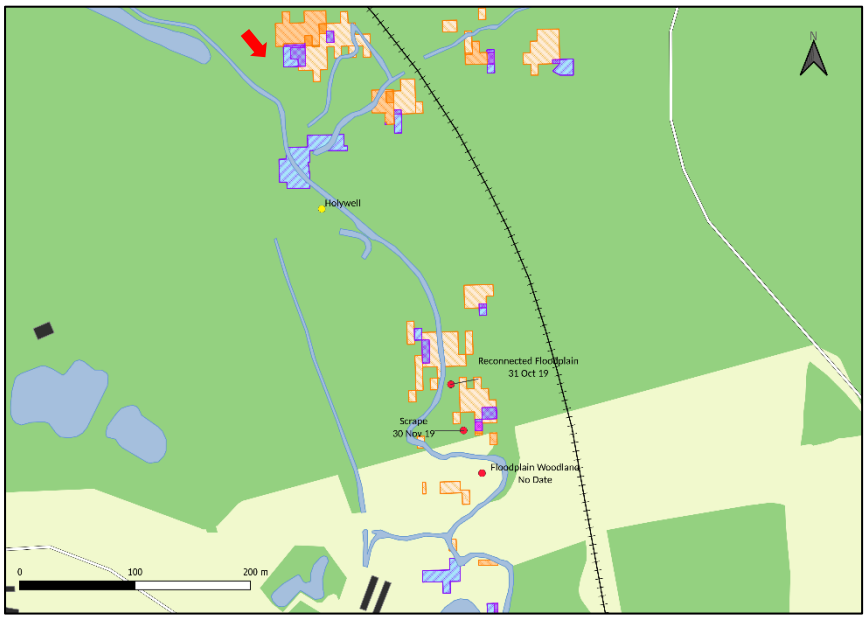

Figure 3.6.10: *Zone 4b –Danehill Brook to Above Cockhaise Mill - Map of flood inundation for pre- and post-NFM events (see key for flood references).*

Figure 3.6.11 below is a photograph of the northern section of Zone 4b, taken from the red arrow position shown on the map extract in Figure 3.6.10. The terrain on the eastern side of Cockhaise Brook up to the railway embankment (obscured by trees) is much flatter and forms part of the original floodplain of the brook.

Figure 3.6.11: *The northern section of Zone 4b showing some of the original floodplain of Cockhaise Brook.*

Figure 3.6.12 below shows a map of the flood inundation around the first group of residential properties, downstream of the NFM installation at Cockhaise Mill in Zone 5. Flood expanses for pre- and post-NFM events are comparable (1.49 ha on 13th January and 1.87ha post-NFM), but again there are very few areas of common inundation.

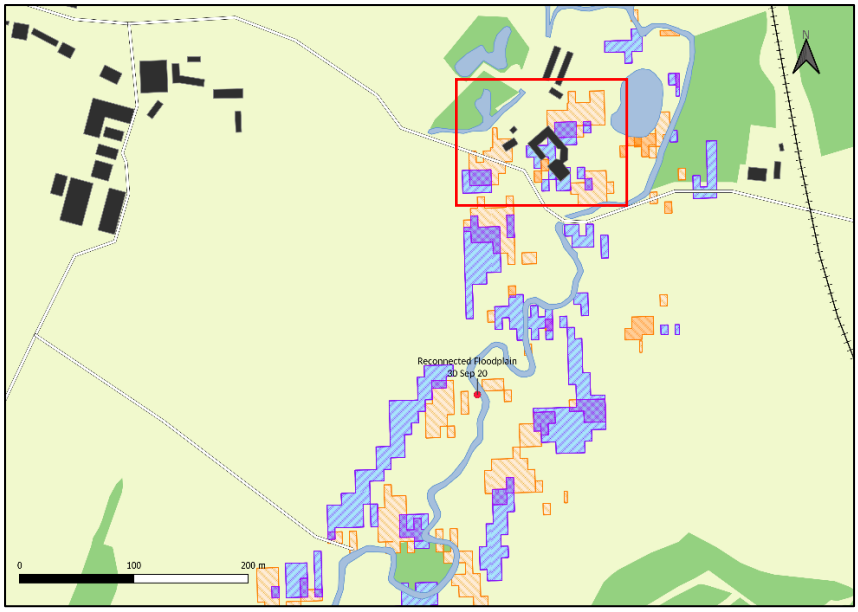

Figure 3.6.12: *Zone 5 – Cockhaise Mill to Freshfield bend - Map of flood inundation for pre- and post-NFM events (see key for flood references).*

Zone 6 is the largest functional zone identified in Figures 3.6.13 and 3.6.14 below and contains the confluence of Cockhaise Brook with the main Sussex Ouse river. This encapsulates a large area of flood, again comparable in size between the 13th January pre-NFM event (2.68ha) and the post-NFM event (3.30ha).

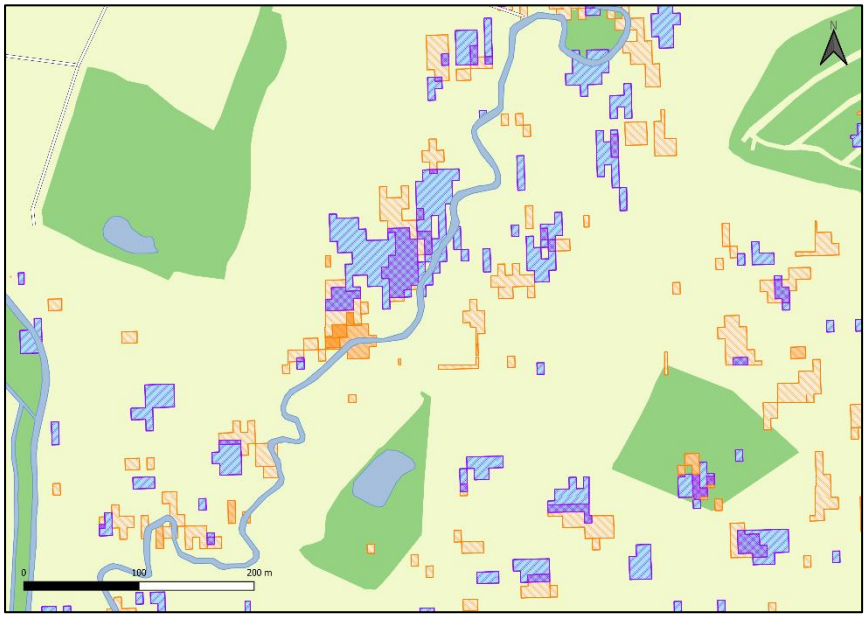

Figure 3.6.13: *Zone 6 – Cockhaise Mill to Freshfield bend - Map of the northern zone section showing flood inundation for pre- and post-NFM events (see key for flood references).*

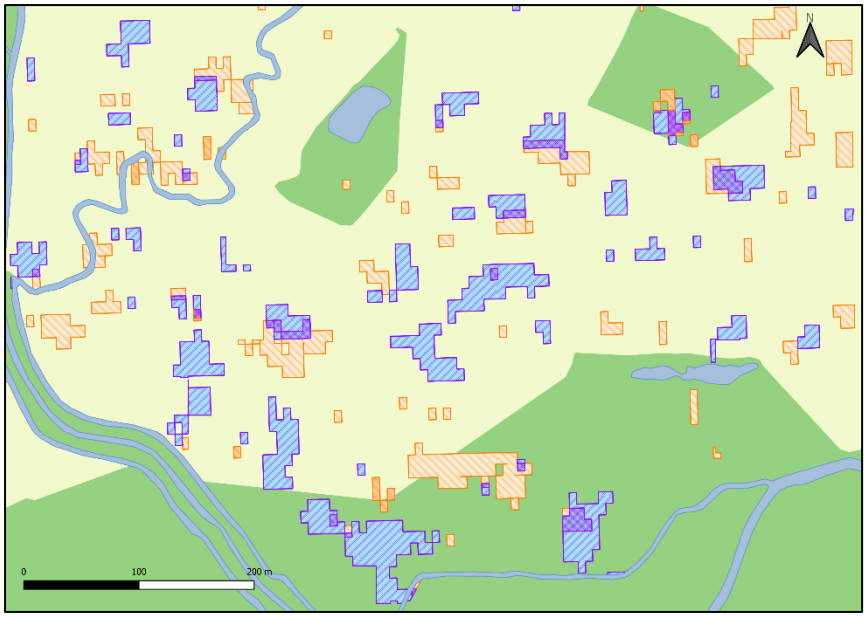

Figure 3.6.14: *Zone 6 – Cockhaise Mill to Freshfield bend - Map of the southern zone section showing flood inundation for pre- and post-NFM events (see key for flood references).*

3.7. Flood Dispersal Results

Incremental 20m buffer rings were constructed in QGIS to measure how far each flood event spread in relation to Cockhaise Brook. A scatter graph in Figure 3.7.1 below illustrates the total area of inundation for the pre-NFM installation flood event between 10th and 13th January 2016 and the post-NFM installation event on 27th November 2019 at incremental 20m distances away from Cockhaise Brook. It is clear from the scatter graph that while the post-NFM flood area was greater (see Table 3.6.1 above), there is a larger concentration within approximately 80m of Cockhaise Brook compared with the pre-NFM flood, but comparable areas at longer distances from the brook.

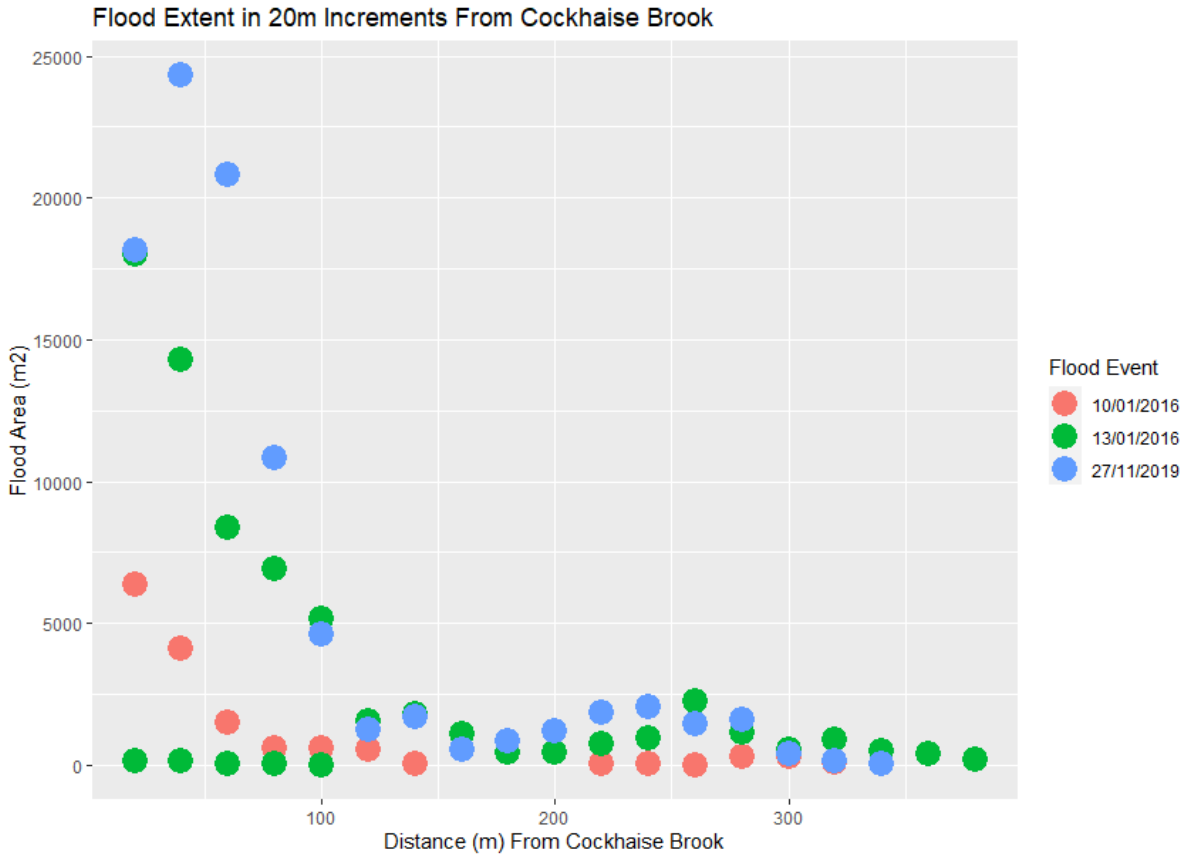

Figure 3.7.1: *Inundated area at 20m increments away from Cockhaise Brook for the pre-NFM flood event in January 2016 and the post-NFM flood event in November 2019.*

The overall dispersal of flooding in each functional zone is summarised below in Figure 3.7.2 using the perimeter length of a convex hull. Again, there is very little difference in size between the flood events, despite the post-NFM inundation being larger in overall physical area occupied.

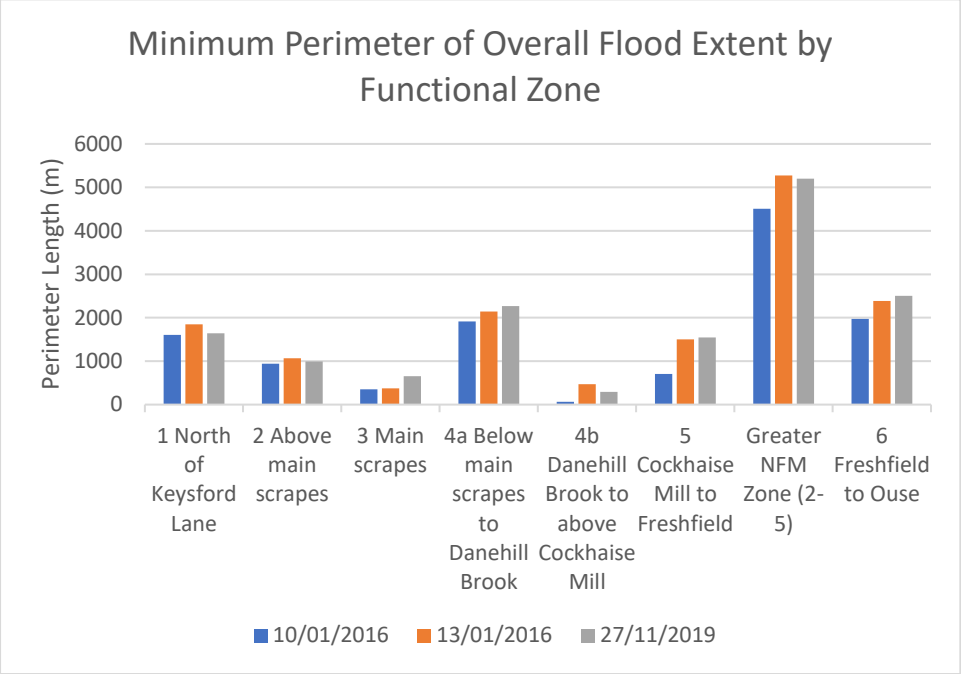

Figure 3.7.2: *Overall flood extent perimeter length for each functional zone based on a GIS-derived convex hull polygon.*

3.8. Flood Extent in Relation to NFM Features

The extent of flood waters immediately around the NFM features was quantified using a single 50m buffer radius around each feature. Figure 3.8.1 below compares the detected inundation for the pre and post NFM events around each NFM feature. The left to right order of the horizontal axis on the graph replicates the positions of the NFM features on Cockhaise Brook, as it runs downstream. The two main scrapes show the greatest increase in flood accumulation post-NFM installation.

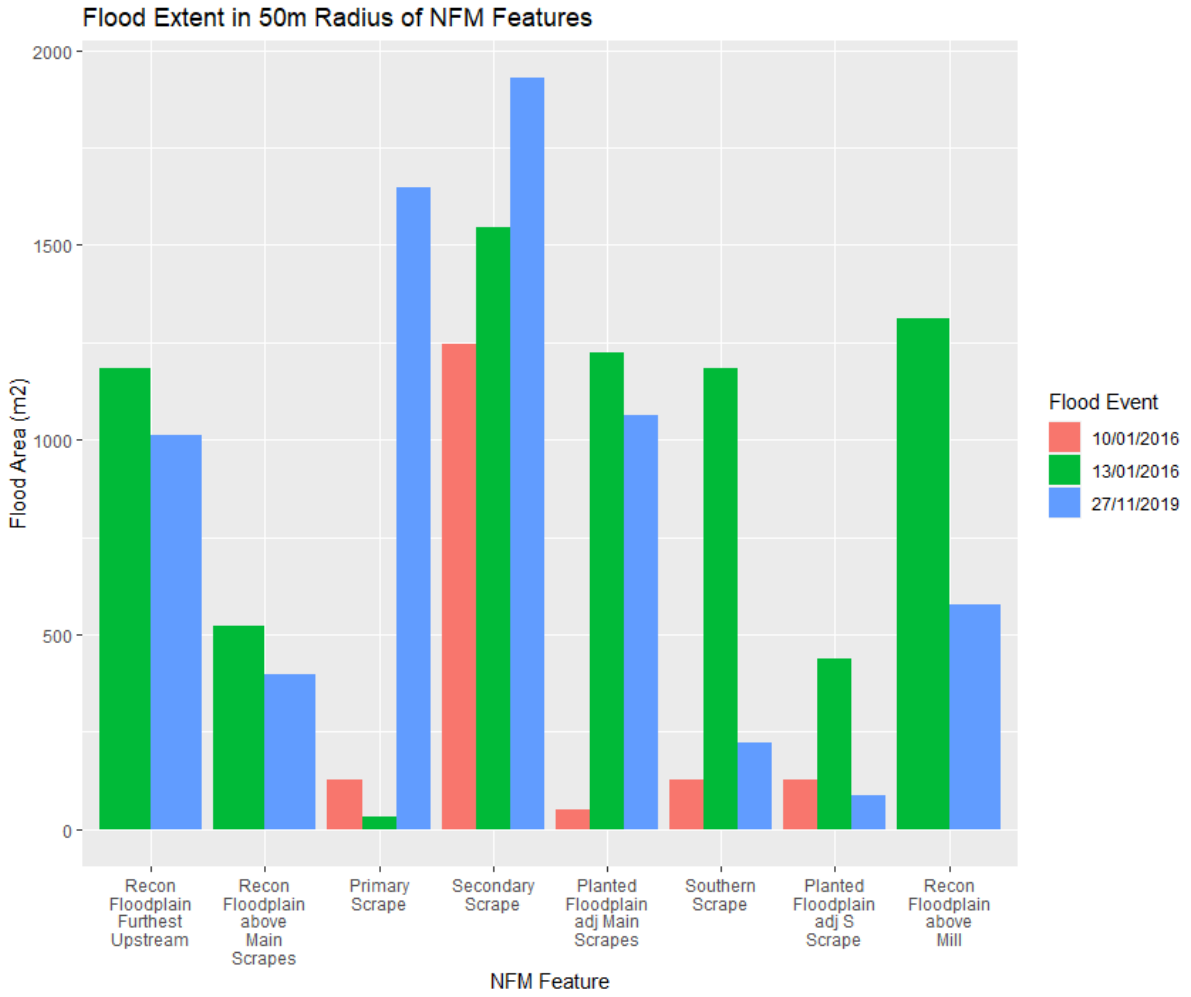

Figure 3.8.1: *Bar chart comparison of the pre- and post-NFM installation flood events by detected inundated area in a 50m radius around each NFM feature.*

3.9. NFM Evaluation Scorecard

Table 3.9.1: *Final evaluation scorecard comparing pre and post NFM flood characteristics of detected area, visually assessed form of flood extent and compactness by zone.*

Functional Zone	Evaluation Criteria					
	Detected Flood Area		Form of Flood Extent		Compactness	
	Status	Positive/ Neutral/ Negative	Status	Positive/ Neutral/ Negative	Status	Positive/ Neutral/ Negative
1 North of Keysford Lane	Increase	Neg	Change	Neg	Increase	P
2 Above main scrapes	Similar	Neu	Change	P	Similar	Neu
3 Main scrapes	Increase	P*	Change	P	Decrease	P*
4a Below main scrapes to Danehill Brook	Similar	P*	Change	Neu	Similar	Neu
4b Danehill Brook to above Cockhaise Mill	Decrease	P	Change	P	Increase	P
5 Cockhaise Mill to Freshfield	Increase	Neg	Change	Neu	Similar	Neu
Greater NFM Zone (2-5)	Similar	P*	Change	P*	Similar	P*
6 Freshfield to Ouse	Similar	P*	Change	Neu	Similar	Neu
Positive Change Score		5/7		4/5		4/4

*Change results judged to be positive in the circumstances of the particular zone assessed.

Table 3.9.1 above sets out the summary scorecard used to evaluate overall change since the NFM installation on Cockhaise Brook against three flood characteristics; detected flood area, form of flood extent and compactness based on the measurements of a GIS-derived convex hull polygon around the flood extent in each zone.

For detected area, five zones achieved positive results in flood extent, including the desired increase around the main scrapes for attenuation purposes. Two zones, north of Keysford Lane and around Cockhaise Mill, displayed negative changes in flood area. Four zones exhibited positive changes in flood extent form, with negative change only in zone 1, north of Keysford Lane. Finally, for compactness four zones recorded positive change, with no changes deemed to have had a negative effect.

4. Discussion

4.1. Optimisation of Histogram Thresholds Using Ground Truth Flood Detection Results

In seeking to obtain optimum flood detection rates using the CDAT process, it can be seen from Table 3.2.1 in the Results section that there is a trade-off between increased detection of flood waters and the risk of including other features with similar backscatter. The trade-off decision therefore is whether increasing flood detection, whilst introducing more false positives is desirable for the phenomenon being analysed. The accuracy assessment employed in this study though considers both aspects with equal weighting to identify optimum settings for processing. Based on the strategy of maximising flood detected in ground truth flood sites and minimising flood detected in dry sites, the best results are recorded in VH polarisation in both weather conditions analysed.

This trade-off is more acute in VV polarisation. It is probable that the increase in false positives (9.8 to 13.3%) and to some degree flood detection (53.4 to 55.6%) in the more windy conditions sensed on 21st December and 20th November, could be the result of sensitivity in VV polarisation to surface roughening of open water such as flood inundation and permanent water bodies (Manjusree et al., 2012). It is interesting to note though that average backscatter values did not noticeably vary for the water bodies sampled across Sussex on the two sets of dates selected for the ground truth analysis, where wind conditions were quite different. Table 3.2.2 shows that for the windy days of 21st December (flood)/20th November (dry), there was a difference of 1.64 Sigma θ DB in VH polarisation against calmer conditions on 20th December (flood)/9th November (dry). In VV polarisation the difference on these dates increased only slightly to 1.95 Sigma θ DB. None of the mean difference values for these water features would have been classified as flood waters using the optimum CDAT settings.

Scatter graph analysis provides another perspective on the relationship between the image date/local peak time lag and detection rates to correctly verify flood waters or mitigate false positive detection. These visualisations of the data illustrate the variance in results of the proportion of flood water detected by polarisation and the river level when the data was sensed, in relation to the flood peak. For dry sites where flooding was not predicted, it is expected that the percentage flood detection will be low to demonstrate the ability of the CDAT method to produce minimal false positives.

The scatter graph for the S-1 image taken on 20th December 2019, (see Figure 3.2.2 in Results section) shows relatively large proportions of flood water/inundation in VV polarisation for Alfriston (28%) and Hellingly (20%). Further investigation of the image difference statistics reveal the standard deviation of backscatter change for Alfriston is noticeably large compared with other dry sites. As houses and roads were included in this ground truth polygon, a possible explanation maybe how VV polarisation could be more sensitive to heterogenous land cover. Sites at Mock Bridge support this explanation, as they also generate a high proportion of false positives (11 and 15%), a similarly large standard deviation and include buildings and roads.

A heterogenous site does not explain the high proportion of false positives at Hellingly though and it is noticeable that this site also posts the largest proportion of false positives in VH polarisation (12%). The issue for Hellingly therefore is not related to polarisation or heterogenous land cover. The probable reason is the lag between the flood image date and the drone footage used to ascertain flood extent and dry areas. It is possible that digitised dry areas derived from the footage may be

inaccurate, as the levels at this point, whilst relatively high as Figure 4.1.3 shows for 27th December, were only 50% of the peak.

Returning again to the scatter graph in Figure 3.2.2, the other dry site at Mock Bridge also has a large proportion of flood water detected in both polarisations (15% in VV and 11% in VH). A factor in this high false positive rate is attributable to errors in interpreting the drone footage. Figure 4.1.1 below shows the flood waters detected on the western side of the site that is very close to the floodplain. The Google basemap shows a line of embankment on which the digitised polygon boundary was based, with possible flood water breaches where cuts in the bank were not visible in the drone footage.

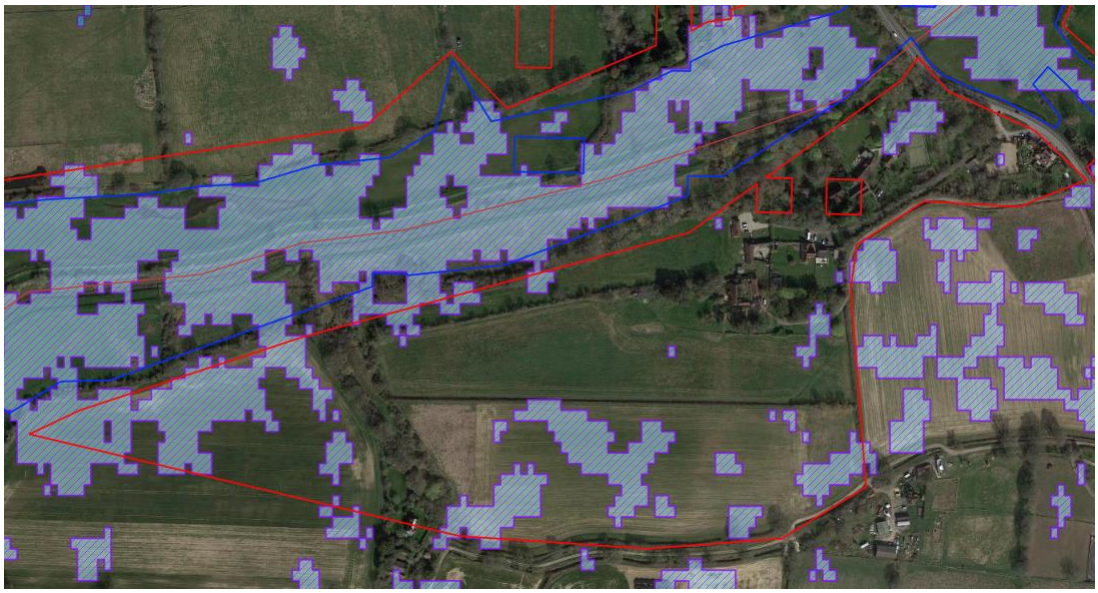

Figure 4.1.1: *A map extract at Mock Bridge, Henfield of a dry site polygon (in red outline) and the concentration of flood waters on the western side.*

For the 21st December 2019, a day after the peak flood on the Sussex Ouse, there is much more variance from the local flood peak. As illustrated in Figure 3.2.3 (see Results section), overall detection of flood waters in dry areas on 21st December is much greater than on 20th December, the largest proportion being mainly in VV polarisation (the site with the largest proportion in VH is the Mock Bridge site highlighted above, where misinterpretation will be a factor in the high percentage). Apart from Mock Bridge, dry area results in VH polarisation are clustered to the left-hand side of the graph, which presents a more acceptable occurrence rate of false positives.

The scatter graphs in Figures 3.2.4 and 3.2.5 (see Results section) of ground truth sites with certainty of total flood coverage on 20th December 2019, should obviously show high levels of flood detection on the right-hand side of the graph. However, they show a dispersed set of results across the horizontal axis in both polarisations. For 21st December in Figure 3.2.5 there is a pattern of low detection rates and higher variance from the time of the flood image to the recorded peak. Mock Bridge and Wineham contradict this as they are geographically very close, but respectively have average flood detection rates of 77% and 15%. This contradiction may be a result of when the drone footage was reportedly captured. For the low detection rates recorded for Wineham, the footage was taken the day before the S-1 image (20th December). Whereas at Mock Bridge footage was taken the day after the S-1 image (22nd December). A possible reason for the low detection rates could be that the flood had significantly receded on the 21st December at Wineham, which is upstream of Mock Bridge on the River Adur.

There are two scenarios affecting the low detection results overall. Firstly, particularly low results on one date, very high results the next day. This is most marked at Alfriston in both polarisations. The probable explanation for this is the difference in timing between the sensed data and the actual flood peak on the river. For instance, Alfriston is on the Cuckmere River, on the eastern side of the ground truth AOI. The nearest gauging station records in Figure 4.1.2 below show the flood rising to a peak on 20th December (the level range on this day was 1.2m) and staying consistently high for the next 2 days (highlighted in green). The S-1A satellite passed at 6am on 20th December, therefore according to these records, capturing the early stages of the flood ascendancy.

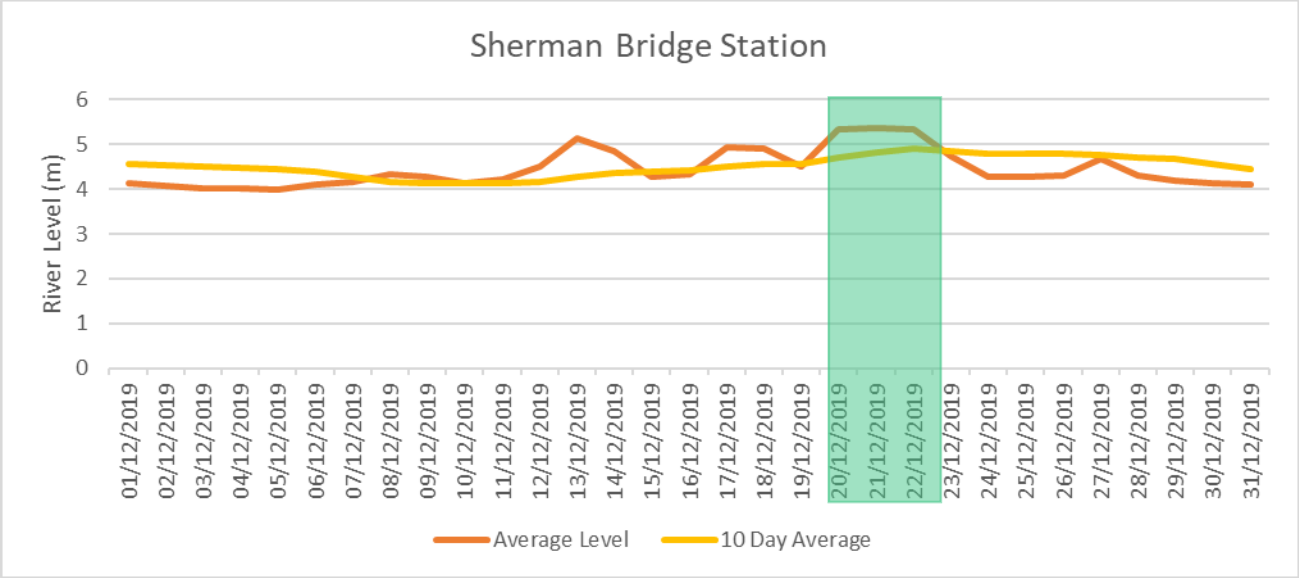

Figure 4.1.2: *Record of average daily levels of the Cuckmere River at Sherman Bridge upstream of the ground truth site at Alfriston in December 2019.*

This may also be the case in reverse at Hellingly on the River Bull, an upstream tributary of the Cuckmere. The local gauging station shows below highlighted in green in Figure 4.1.3, a sharp drop in river levels after the peak on 20th December, resulting in low detection rates on 21st December.

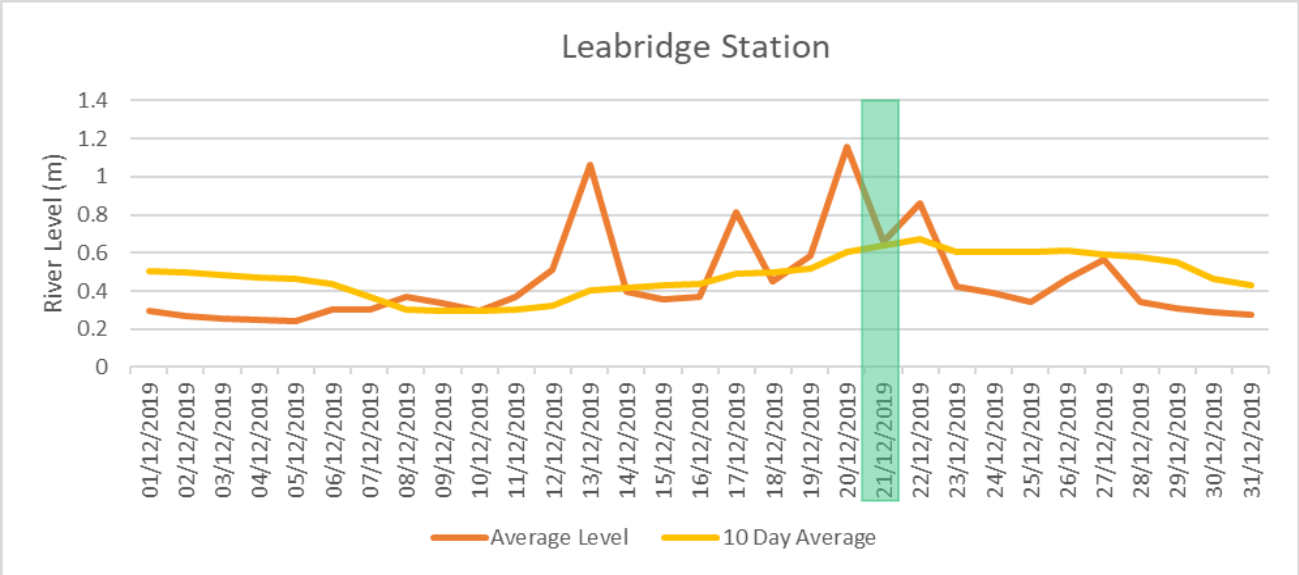

Figure 4.1.3: *Record of average daily levels of the River Bull at Leabridge upstream of the ground truth site at Hellingly in December 2019.*

At Walstead, the nearest site to the NFM features themselves, the scatter graphs in Figures 3.2.4 and 3.2.5 of the Results Section show very high detection rates on 20th December (91-96% in both polarisations) on the right-hand side of the graph in lilac, but very low rates on 21st December (17-41% in both polarisations), at mid-level to the left-hand side. Local river level records though indicate that the flood had receded by 50% the day after the 20th December peak, as highlighted in green in Figure 4.1.4 below.

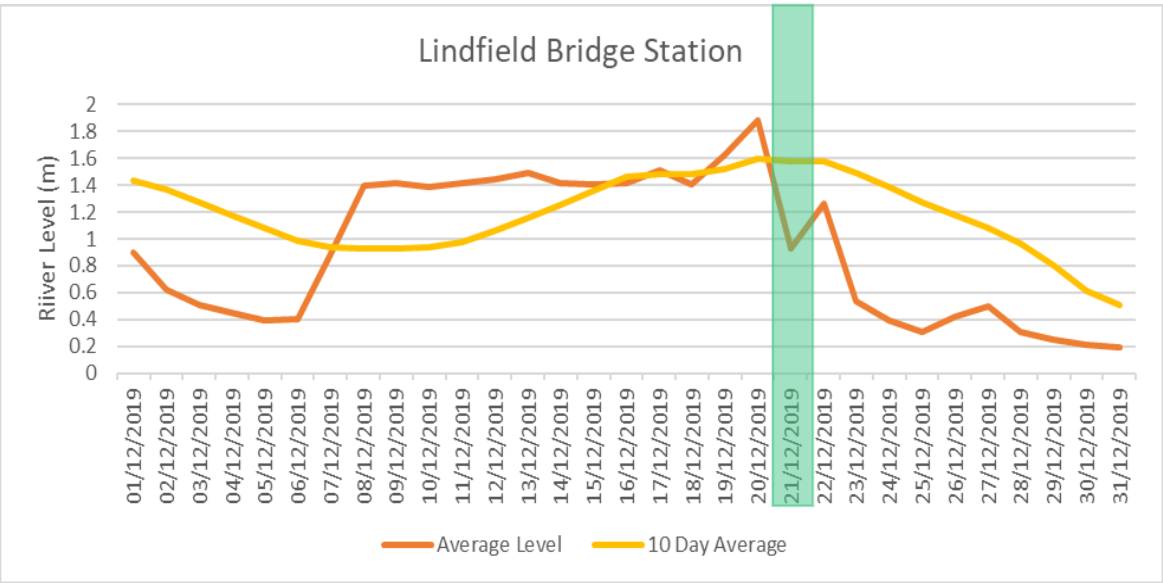

Figure 4.1.4: *Record of average daily levels of the River Ouse at Lindfield Bridge upstream of the ground truth site at Walstead in December 2019.*

It can be seen therefore that a major characteristic of fluvial flooding in Sussex is the sharp recession of waters after the peak event, as demonstrated on the Cuckmere River at Alfriston, its tributary the River Bull at Hellingly, the River Adur at Wineham and the River Ouse at Walstead, near to the NFM installation. Therefore, of paramount importance to flood image selection is the time lag with the peak level flood of the river being monitored.

The second scenario is consistently low detection levels on both dates. The Wineham site achieves the lowest (14-46% in both polarisations over both days). A possible explanation is the relatively high 10-day average level of the River Adur at Sakeham Weir gauging station on the baseline dates shown in green in Figure 4.1.5, which is 1km downstream of the Wineham ground truth site. Whilst the site at Mock Bridge is only 250m further downstream of Sakeham Weir, the weir itself by its very nature inhibits flow, which may manifest in the river banks upstream at Wineham being breached, or at least increased ground water levels on the reference dates.

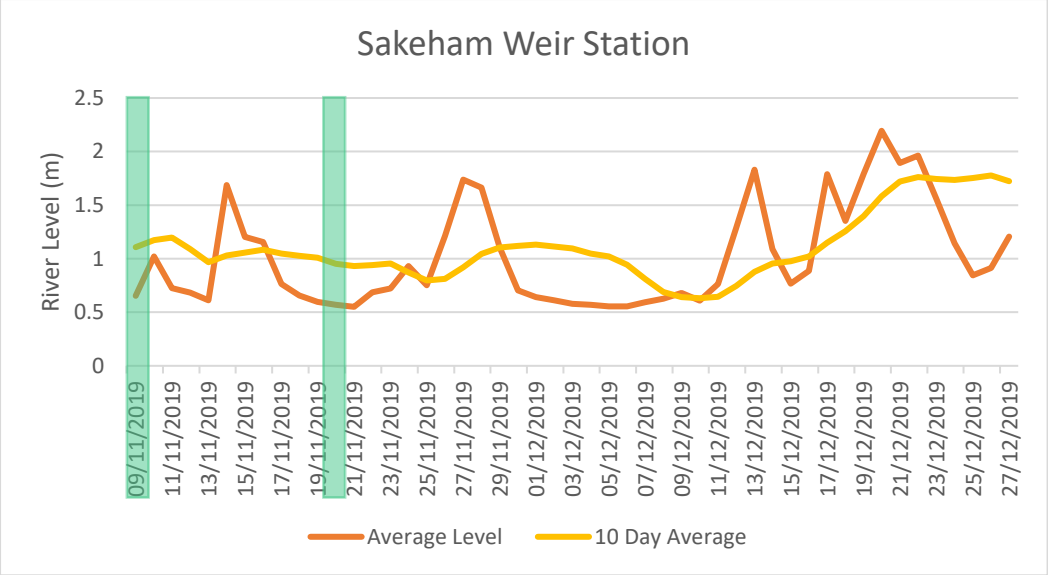

Figure 4.1.5: *Record of average daily levels of the River Adur at Sakeham Weir between the ground truth sites of Wineham (upstream) and Mock Bridge (downstream) in the period from the reference date of 9th November 2019 and the ground truth flood coverage derived from drone footage taken between 20th and 22nd December 2019.*

If backscatter returns for the reference dates were low at that time due to the presence of flood water or very wet ground conditions, this will hamper change detection as the difference with the flood date values should produce a result that is outside of the histogram zone, representing open flood water. To be credible, this reasoning would require the backscatter average where flood hasn't been detected to be noticeably high on the reference date. For ground truth sites representing known flood areas, Figure 4.1.6 below shows the difference between the flood and reference image backscatter returns for the 20th December S-1 image, but in locations where no inundation was detected. Hence, this is why the difference is positive. For these areas, backscatter returns had increased between the reference and flood image date, when if they were actually flooded, radar returns should have reduced, thereby resulting in a negative difference. This increase though is not due to bounce caused by branches or grasses, as inundated vegetation displays a more significant increase than those recorded for these areas. The standard deviation of the flood and reference images in each site has been included in Figure 4.1.6 to highlight the variance in backscatter for each site.

Apart from Alfriston, for which reasoning has been presented above, Wineham displays the highest difference and overall, the third lowest standard deviation in the reference image. These metrics are not significant in relation to the other sites, but do not contradict the possibility that latent flood waters in this area could be the cause of the low detection rates found at Wineham. Allied to this, according to British Geological Society records, the soil type at Wineham and Mock Bridge is Weald Clay. Apart from the small site at the Anchor Inn, the other sites are on better draining soils (Alfriston is on chalk, Hellingly on Tunbridge Wells sand), where ground conditions in winter will be relatively drier compared with Wineham and Mock Bridge.

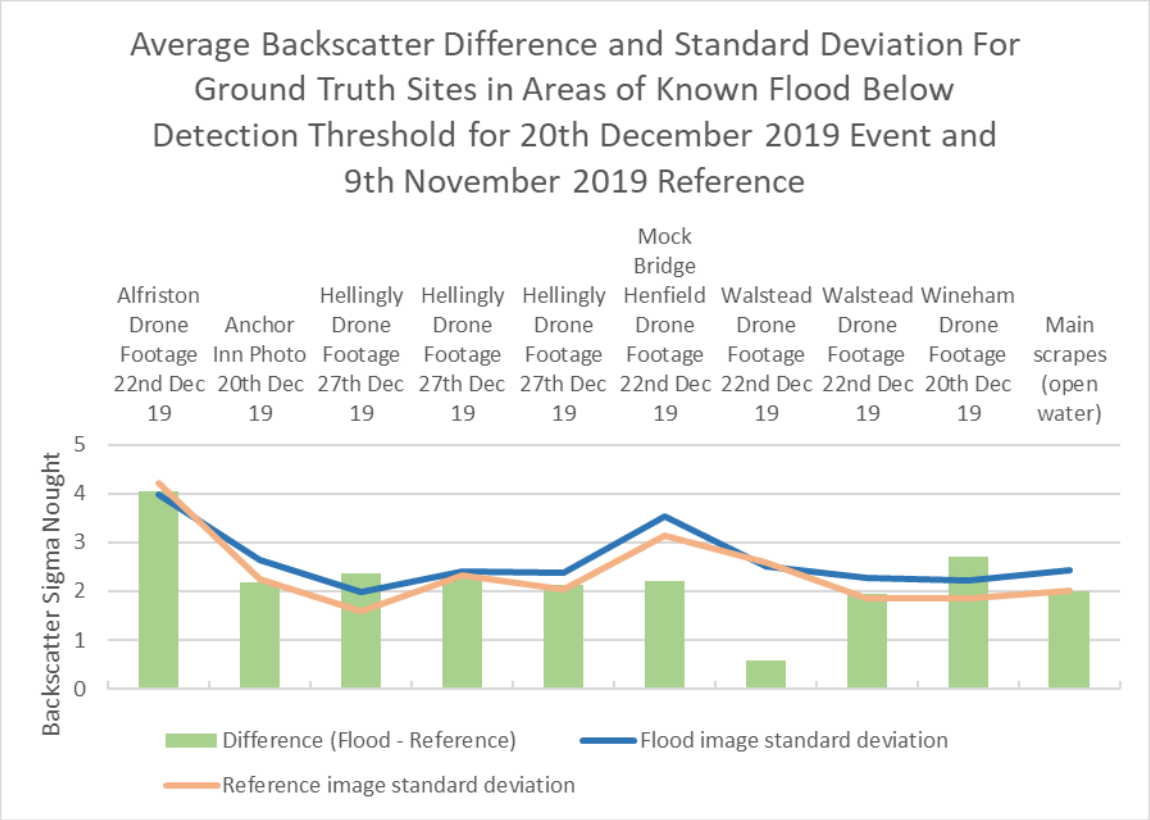

Figure 4.1.6: *Average backscatter difference and standard deviation for 20th December 2019 flood and 9th November 2019 reference images in ground truth sites with evidence of flood where below detection threshold.*

Therefore, for Wineham, the possible effects of Sakeham Weir on local fluvial flooding presented complicates a comparison with the opposite results gained at Mock Bridge. However, in considering the causes for these low results the argument that the peak flood was already receding at 6am on 20th December is not correct as the river level records in Figure 4.1.5, the results for nearby Mock Bridge and the drone footage all demonstrate. The argument that the area was already saturated is plausible, especially with the different soil conditions identified, but in comparison to radar backscatter in other sites as Figure 4.1.6, it is not compelling evidence. The local effect of the weir aside, Mock Bridge also contradicts this explanation.

At 21ha, the Wineham flood site constitutes approximately 20% of the total ground truth area for known floods. Therefore, these low rates for the site heavily skew the overall proportion, especially on 21st December, in which flood water detection was only 14% in VV and 16% in VH polarisation. The inconclusive results of the more in-depth analysis conducted at Wineham for the low rates on both dates, prevents a reasoned argument as to their removal from the overall ground truth totals upon which accuracy assessments have been calculated. This then brings into question the choice of a large variance in size of the ground truth sites. Similar sized sites would not have skewed accuracy results in such an acute way, if anomalies such as Wineham occurred.

4.2. Optimum Histogram Threshold Settings

To determine the most accurate histogram threshold settings for application in the change detection analysis, a range of coefficients were used to classify the ground truth flood/dry difference image. Figure 4.2.1 below again uses the histogram of difference values for the 21st December 2019 flood and reference of 20th November 2019 dataset to illustrate how the selection of coefficients affects the thresholds determining the statistical zones representing flood and inundated vegetation. The mean difference value is shown with the red line, one standard deviation away from the mean is shown with the green lines. The orange lines depict the optimum threshold settings from the results of the accuracy assessment. These use coefficients of 1.2/1.3 for open flood waters and 2.5 for inundated vegetation. According to the CDAT method, pixel values to the left of the lowest orange line are open flood waters. Those to the right of the highest orange line are deemed inundated vegetation. It can be seen that there are much less areas of inundated vegetation compared with those in the open water flood zone. The purple lines illustrate what happens when these coefficients are adjusted. The lowest purple line decreases the amount of flood water detected by increasing the coefficient value to 1.5. It could though also reduce the number of false positives. The highest purple line increases the amount of inundated vegetation detected by reducing the coefficient value to 2.3. However, this could also increase the number of false flood positives in dry areas.

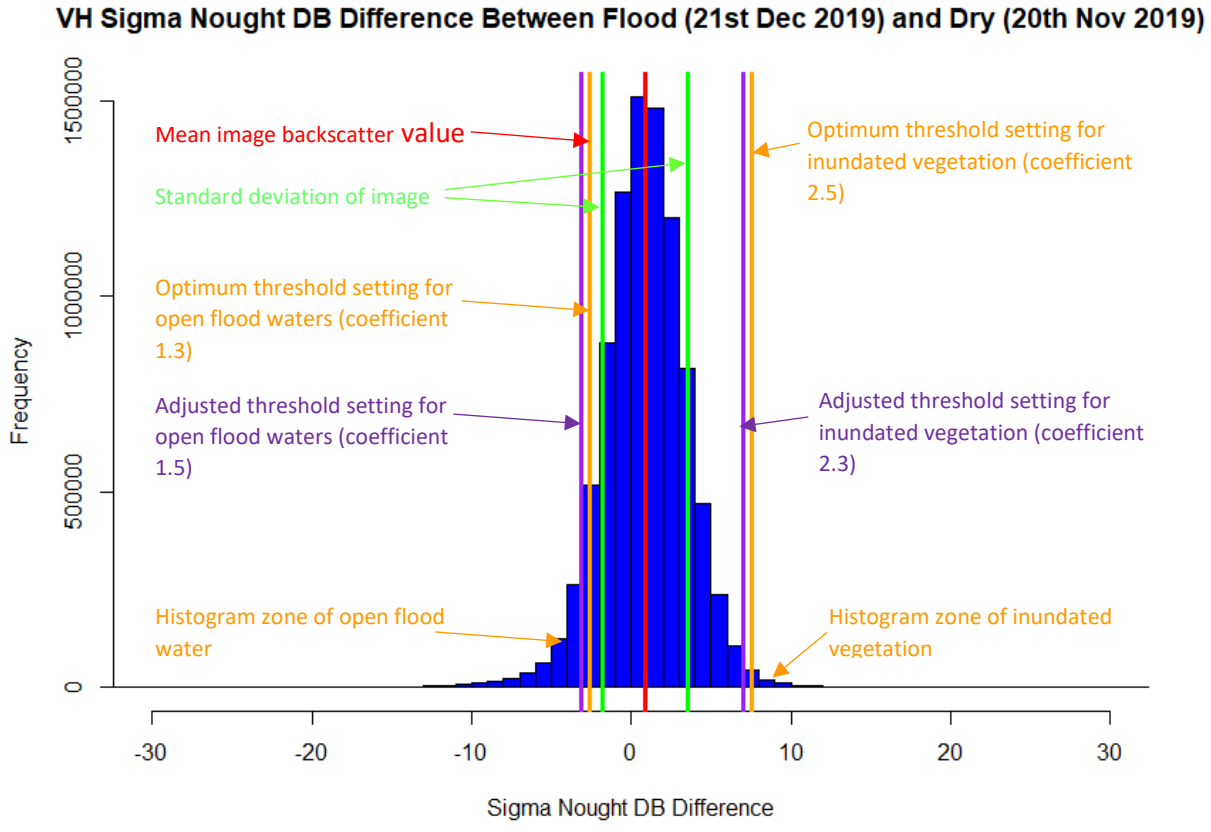

Figure 4.2.1: *Histogram of Sigma∂ dB values for the difference between the flood image of 21st December 2019 and dry image of 20th November.*

The results of the accuracy assessment of ground truth sites have been used to dictate the histogram threshold settings for detection of flood waters on Cockhaise Brook. A CDAT method in VH polarisation using coefficient values of 1.3 and 2.5 to detect open flood waters and inundated

vegetation respectively achieved the best Kappa statistic, a 48% better outcome than random classification (see Results – Table 3.3.1). These settings though do not provide a very reliable detection rate for the NFM evaluation, especially as the problem is the underrepresentation of flooding. False detection of flooding was only 9%.

There are some important considerations to make in assessing the reliability of the CDAT method based on these results. The factor with the biggest impact on confidence, but with the least basis to make any adjustment is the Wineham ground truth flood site detection rate. For such a large site, only 16% of flood waters were detected. Removing these results would increase the overall detection rate from 57 to 67% and the Kappa Statistic to 50%. Adjustment of dry ground truth site boundaries where shown to be inaccurate, may further slightly improve the Kappa Statistic. Digitising more homogenous land cover on ground truth sites may also be beneficial, as this may also affect detection rates, especially in limiting false positives.

The fundamental conclusion to draw from the accuracy assessment is that in VH polarisation the detection of flood water is marginally better than in VV in windy conditions (see Results Tables 3.3.1 and 3.3.2, 56.5% and 55.7% respectively). VV polarisation is marginally better in calmer conditions (see Results Tables 3.3.4 and 3.3.3, 52.5% and 52% respectively). However, in both conditions there are more false positives in VV polarisation, therefore reducing overall accuracy below the results in VH. On this basis, VH is the most beneficial polarisation to use in both calm and windy conditions.

Another positive outcome from the accuracy assessment is that the rates of false detection in both polarisations and in windy or calm conditions was consistently low at 6 to 13% (see Results – Table 3.3.1 to 4). The main issue therefore is low rather than incorrect flood water detection. The impact on the evaluation therefore is an underrepresentation of flood extent, rather than inaccurate representation.

4.3. Evaluation of NFM Features Using Optimal Coefficient Settings

4.3.1 Flood Area and Location

The analysis results for the evaluation of the NFM installation require that the stacked bar chart of flood inundation area by functional zone for the pre- and post-NFM flood events in Figure 3.6.1 of the Results section is cross-referenced with the zone maps shown in Figures 3.6.4,6,7,9,10,12,13,14 to understand how the spatial form of flooding on Cockhaise Brook has changed. Zone 1 is furthest upstream of the NFM installations. Flood waters to the north of Keysford Lane have increased from approximately 0.5 hectares in the ascendancy/descendancy stages of the pre-NFM event to over 2 hectares post-NFM. This is a substantial change that is not readily explainable by attributing to the effects of the NFM features. Indeed, the negligible change in flood area in Zone 2 immediately above the main scrape features rule out any negative effect of the main NFM installations. Potential agricultural land use changes around the northern section of the brook since 2016 could explain this change in flood form, with possible run-off from the slopes on either side of the brook.

The stacked bar chart in Figure 3.6.1 captures a general lack of coincident inundation between the pre-NFM and post-NFM events. Looking at this lack of coincidence in more detail, the area with least commonality between pre- and post-NFM flood inundation was Zone 4a, immediately below the main scrapes (see Results – Figure 3.6.9). Only 3% of the total detected area of flood in this zone coincide between the pre- and post-NFM events. 44% was detected only in the post-NFM event and 53% in the combined pre-NFM event (aggregated 10th and 13th January areas). Therefore, it can be summarised that the flood area decreased post-NFM in 4a, with a substantial shift in location as shown in the zone map. The brook flows in a north-east to south-west direction through Zone 4a. In

the north-east corner, up to immediately after the confluence with a small stream (marked with the red rectangle), there is a strong case that the reason for much less post-NFM area compared with the pre-NFM flood is the effect of attenuating flood waters in the main scrapes in the adjoining upstream zone. Whilst the nett area of 0.2ha for pre-NFM flooding in this part of Zone 4a is small, there is good evidence that this is a tangible effect of managed inundation.

The second lowest coincidence of pre- and post-NFM flood area (6%) is in Zone 2, interestingly immediately upstream of the main scrapes (see Results – Figure 3.6.6). Therefore, both zones adjacent to the main scrapes display the least proportion of coincident areas of detection. 59% of the total flood area detected in Zone 2 was for the pre-NFM flood, 35% post-NFM. Again, there has been a reduction and shift in flood area. The map of Zone 2 shows pre-NFM flooding in a much more dispersed pattern than the more concentrated inundation of the post-NFM event that clusters around the brook itself. This correlates with the buffer ring analysis in the scatter graph shown in Figure 3.7.1, which depicts a pattern of post-NFM flood waters being more closely situated to the brook. It is interesting to note that these evaluation interpretations for Zone 2 do not concur with the positive view of the SFI Project Manager S. Buckland. In his view, inundation shown pre-NFM was not a regular occurrence in this area from SFI observations prior to installation works (personal communication, 16th August 2022). The project considers the water accumulation here to have been a tangible success of managed change in functionally re-engaging the floodplain. In this instance, comparing flood peaks rather than periods of higher flow levels may mask how the brook operates the majority of the time post-NFM, in using the floodplain. According to S. Buckland this did not occur previously (personal communication, 16th August 2022).

The pre- and post-NFM floods correspond most closely where the main scrapes are situated in Zone 3 (see Results – Figure 3.6.7). 18% of total flood area detected was coincident for both events. 53% was detected only in the post-NFM event and 27% only in the pre-NFM event. In this zone, flooding has increased post-NFM and as borne out in the high prevalence of flood waters within a 50m radius of the primary scrape in Figure 3.7.2 and illustrated in the map, has been generally diverted into a concentrated managed space.

Zone 5, the area immediately around Cockhaise Mill up to Freshfield bend (see Results – Figure 3.6.12) is where the NFM measures were designed to have their most substantial impact. 10% of the flood inundation detected for this zone remained unchanged between the pre- and post-NFM events. However, there is proportionally more flooding overall in Zone 5 post-NFM (49% compared with 41%). Aside from the aggregate sum used for the two pre-NFM flood extents, some context is required in relation to this comparison. Figure 4.3.1 below shows the area around the mill buildings in more detail, with shaded relief included for an understanding of the local topography. The SFI Project Manager S. Buckland cites pluvial surface water flow from higher ground running down to the mill buildings also being detected in the CDAT results (personal communication, 16th August 2022). The blue arrows in Figure 4.3.1 show how surface water flows from higher ground and accumulates around the mill buildings. This source of flooding is outside the scope of the NFM measures and may skew results to some degree. Inundation is also mostly concentrated in the southern part of the zone running parallel with the brook, generally away from the mill buildings. The linear form of the post-NFM flooding running parallel to the brook on its northern bank is probably related to the reconnected floodplain forming part of the NFM installation.

Focusing though on the area immediately around the mill buildings, as the red rectangle in shown in Figure 3.6.12 and at larger scale in Figure 4.3.1 below, there is less flooding post-NFM. Taking into account the surface water flow issue, greater emphasis should be placed on the area most susceptible to fluvial flooding between the south-western side of the mill buildings and the brook,

where it can be seen that post-NFM inundation extent has also improved. Awareness is required of surface water flow from higher terrain running across lower-level impervious surfaces, such as in this scenario, as these sources of flood may be outside the design scope of a catchment-scale flood management solution.

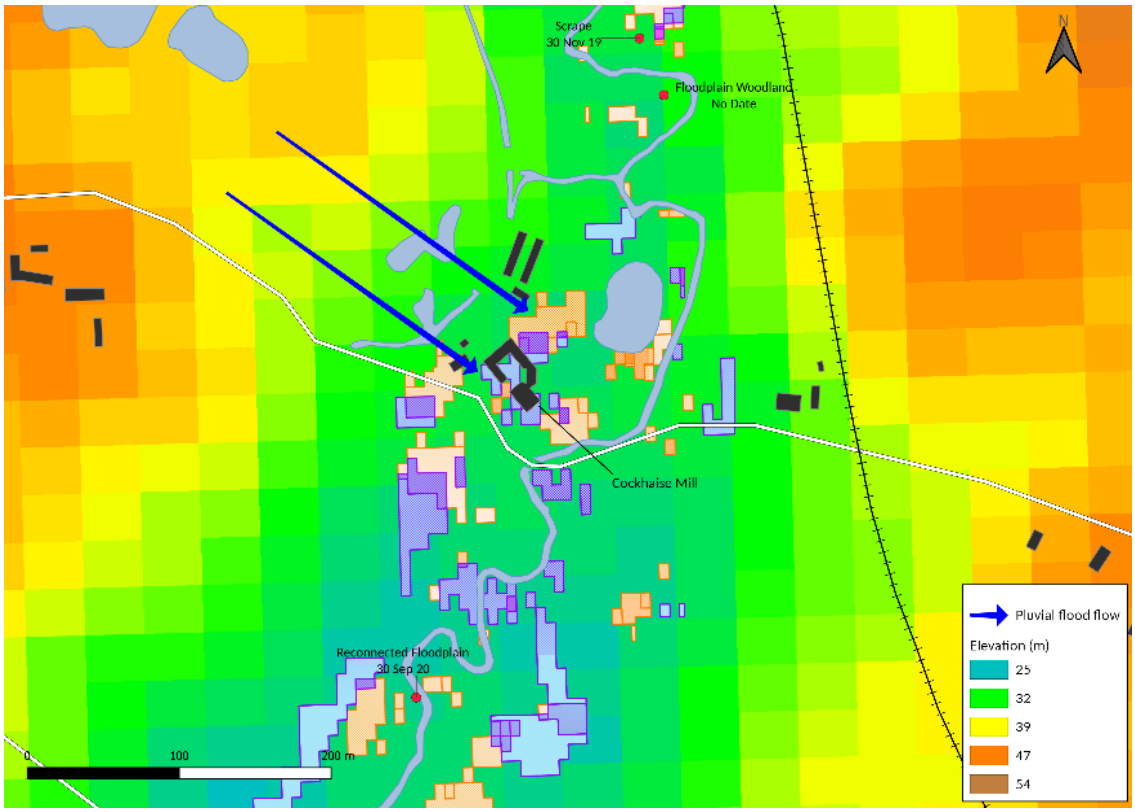

Figure 4.3.1: *A larger scale map extract at Cockhaise Mill showing terrain and surface water flow from higher ground.*

Zone 4b immediately upstream of Cockhaise Mill up to the Holywell weir (see Results – Figure 3.6.10), displays a large difference in flood characteristics. Pre-NFM flood waters account for 87% of the zone total detected, with 9% coincident between the events and only 4% in a different location post-NFM. Therefore, it can be summarised here that flood waters have greatly reduced in the area immediately upstream of Cockhaise Mill.

In considering Zones 4b and 5 in combination, there is a possible aggregate effect of the main scrapes and nine other NFM features in these zones or immediately upstream changing certain flood characteristics on this section of Cockhaise Brook. Flooding has reduced around Cockhaise Mill and immediately upstream by 0.5ha in area. Flood area has also decreased by 24% in Zone 2, immediately upstream of the main scrapes.

These results, together with the doubling of flood attenuation generally concentrating around the main scrapes in Zone 3 (27 to 55%) post-NFM, provides a firm basis to propose that NFM measures have changed the flood characteristics of Cockhaise Brook. In aggregate it is clear that the introduction of NFM installations has reduced flooding where intended and attenuated inundation in managed spaces, generally in line with the design intentions.

4.3.2. Flood Dispersal

Changes in dispersal after NFM installation on Cockhaise Brook in Figure 3.7.1, clearly show how the vast majority of flood waters remain in close proximity to the flood source compared with the pre-NFM event. Within 20m of the brook, flood area is very similar. However, the blue points at distances 40, 60 and 80m from the brook, illustrate how over 26,000m^2 of flood waters accumulate more closely to the brook during the post-NFM event. The trend after these distances then broadly correlates with the pre-NFM event. This provides clear evidence how post-NFM, the pattern of flood relates more closely to the linear form of its source i.e. Cockhaise Brook.

However, is this spatial form what was intended in the design of the NFM installation? Whilst inundated areas may be closer to their source, this may be detrimental to general land use of the area. What must also be considered is the topographic context as to how a flood is managed. In this situation, care has been taken to use the indicator where there is no large expanse of floodplain, allowing greater dispersal that may be considered a desirable outcome. There are also no buildings or infrastructure prior to the mill buildings at immediate risk of flood.

4.3.3. Flood Extent in Relation to NFM Features

By taking into consideration detected inundation around NFM features, there is a clear indication that the closer proximity of flood waters to Cockhaise Brook in the post-NFM event is a designed outcome. Figure 3.8.1 in the Results section shows how flood waters of over 1,500m2 were detected within a 50m radius of both main scrape features. The primary scrape especially has provided substantial additional functioning floodplain capacity that was not available prior to the reconnection works. Flood extent has decreased in the post-NFM event immediately around reconnection points to the floodplain upstream of the main scrapes. This could reflect the greater capacity of the scrapes lessening flood flow at these locations.

The southern scrape is an anomaly compared to the evident concentration of flood waters in the main scrapes further upstream. An early iteration of the mapped extent of the 27th November 2019 event did not detect any flood waters around the scrape. The CDAT operation was based on the reference date of 20th November 2019, which as shown in Figure 2.3.2 of the Methodology Section was specifically selected as the brook was at a relatively low level (daily average 0.15m compared with the flood peak of 1.77m). Without taking into account wind conditions, this was considered to be the optimum difference in river level compared with the 27th November flood event. However, negligible change was detected using these images. These findings were conveyed to S. Buckland, the SFI Project Manager, who observed that the scrape in question was dry in April 2022, whilst the main scrapes were still attenuating run-off (personal communication 26th March 2022). The CDAT operation used for the final analysis references data from 9th December, to mirror the strong wind conditions at the peak of the flood on 27th November. This also detected very little change in backscatter between the two dates. Therefore, the possible explanations of slow drainage of the scrape or greater backscatter caused by wind disturbance of flood waters have to be largely ruled out. A simple explanation may just be the smaller size of the scrape in relation to the spatial resolution of the SAR imagery.

Planted areas of the nationally rare Black Poplar tree have been included in the assessment of NFM features as they have a slowing effect on floods in addition to their biodiversity function and water cleansing properties. These features will take a longer time period to provide tangible evidence of flood management benefits, as the woodland establishes itself and explains the differing levels of flood waters detected in their immediate vicinity in Figure 3.8.1 of the Results section.

Overall, the detected concentrations identified with the 50m buffer zone analysis attenuate flood waters most markedly in the main scrapes. Other features were possibly too small, or in the case of the planted woodland, less relevant in attenuating flood waters.

4.3.4. NFM Evaluation Scorecard

The scorecard results provide strong evidence of beneficial changes in flood characteristics after the installation of NFM measures on Cockhaise Brook in terms of; detected area, the form of inundation and the compactness of overall zonal extent.

4.3.4.1. Detected Flood Area

Area comparison has been based on an aggregated pre-NFM total, which may not reflect the actual peak flood event. Despite increased attenuation being introduced to the brook, the greater region of Zones 2-5 does not display more flood water area. This was also the case individually for Zones 4a and 6, where the post-NFM peak did not generate any greater area of detected flood waters compared with the descending pre-NFM event. However, this was not the case for Zone 2, which contains NFM measures and would therefore expect an increase in area, especially when considering the assimilate comparison between the pre- and post-NFM events.

Negative changes were identified where there were increases in detected area in zone 1 north of Keysford Lane and in Zone 5 around Cockhaise Mill. As previously discussed, there are no obvious reasons for these changes, other than the surface water issue in Zone 5 as observed by S. Buckland of the SFI, but this must be taken into account in the overall evaluation. Increases in flood water area overall in Zone 5 must be considered in relation to the reduction immediately around the mill buildings, as the key aim of the SFI project is attempting to reduce flood risk in this location. Also, taking account of the other characteristics evaluated (form of extent and compactness) and the surface water issue identified, the overall evaluation for Zone 5 results in a more neutral outcome. Where these flood waters are situated, despite there being more area, is no more detrimental for the residents of Cockhaise Mill overall. Also, again it is worth considering that more flood water area covers a similar overall extent in comparison to the pre-NFM event.

4.3.4.2 Form of Flood Extent

Overall, visual analysis of each zone is generally favourable as to how inundation has concentrated in areas containing NFM features. This is supported in the scorecard, with four positive changes observed. Figure 3.7.1 in the Results also verifies how inundation has remained very close to the brook.

The only negative outcome in terms of form of flood was for Zone 1 north of Keysford Lane. Here, inundation extends into adjacent agricultural fields and is concentrated very close to the road.

4.3.4.3 Compactness

In terms of compactness, flood water extent, despite more area, has remained relatively similar. Even Zone 1, where changes have been interpreted overall as less favourable, compactness of the flood has improved. Converse to the other verdicts on compactness, Zone 3 containing the main scrapes is less compact, but as this reflects the NFM design intent, a positive change has been acknowledged.

Overall, the scorecard provides a balanced interpretation that positive change has resulted from the introduction of NFM features on Cockhaise Brook. For all three indicators; flood area, flood form and

the compactness of the inundated extent, positive change has unequivocally outweighed the negative outcomes identified.

4.4. Sussex Flow Initiative Use of Results

Close contact with the SFI Project Manager S. Buckland was maintained throughout the research process. Feedback was obtained at key stages to provide context on how the delineated flood maps relate to anecdotal experience when flooding has occurred and the design intentions of the project.

Research results have been included in the SFI annual report for 2021/22 (SFI, 2022) citing how the area of attenuation around the main scrapes in Zone 3 has been captured as functioning in accordance with design intentions. From their own depth records, SFI augmented the research in converting the accumulated flood waters to a storage volume. Water storage capacity is the key functional metric used in the NFM domain. Whilst a site survey of the constructed scrape can provide the volumetric attributes of a scrape, remotely sensed data in peak historical flood conditions, as carried out in this study, provides evidence of the scrape performing its inundation management function in response to the most testing events. The SFI Project Manager S. Buckland cited 'the value of remote sensing to show changes in function' during feedback exchanges (personal correspondence, 16th August 2022).

4.5. A Critique of the Study Methodology

In reflecting on the results of this study, sound project management principles demand that a critique be undertaken on the methodology employed. Each aspect of the study structure has therefore been assessed, to identify areas of improvement and adaptation to widen the relevance of the research.

4.5.1. The Study Area

Whilst the SFI project is a driver in establishing wider use of NFM techniques, it is fair to say that it is small-scale and exploratory in its goals. This experimental approach has made its evaluation a more subjective process. The small scale of the catchment and the areas of flood inundation have also required more subjectivity in assessing the effects of the NFM measures. The cases of the surface water issue around Cockhaise Mill and the lack of attenuation found at the southern scrape, are examples of the analytical limits of the study due to the spatial resolution of the data used. However, the inclusion of early research findings in the project annual report, indicate that this methodology is relevant in providing research evidence of what NFM installations can achieve and how they affect flood characteristics in critical events.

4.5.2. Remote Sensing Technique

There are many proven remote sensing flood index techniques delineating extent that could have been used to analyse the changes in form and area of events pre and post NFM installation. Established indices such as the Modified Normalised Difference Water Index (MNDWI) using optical imagery provide robust results (Xu, 2006). However, change detection seeks to minimise external differences to maximise identification of a phenomenon, in this instance flood waters, in relation to the seasonal characteristics of an AOI. Replicating the methodology of Long et al (2014) using the CDAT technique, provided a suitable workflow for other flood management projects, in terms of its portability and elementary approach. Use of the more complex HAND GIS procedure as the methodology of Clement et al (2018), may have provided a more nuanced mask of where flood waters accumulate on a small catchment, such as Cockhaise Brook. Further research would certainly be worthwhile in testing a HAND mask against the slope mask employed in this study.

4.5.3. Data

Greater spatial resolution could have been achieved with more budgetary resources. For example, TerraSAR-X satellite data provides 1m resolution in the X-band microwave frequency, which is suitable for flood detection. This would certainly have suited the small-scale catchment of Cockhaise Brook. However, the temporal resolution of 6 days for the S-1 data proved invaluable in being generally able to capture the short window of flood peak on the brook. This would have been much more problematic with lower temporal resolution imagery (TerraSAR-X resolution is 11 days).

4.5.4. Flood Selection

Key to the CDAT methodology employed in this study, was the selection of seasonally-similar datasets. River level records show comparable flood peaks for a post-NFM scenario in January 2020, against the selected scenario of January 2016 pre-NFM. However, this would compare S-1A and 1B images and a 50% greater 10-day river level average. The trade-off benefit though would have been very similar seasonal flood scenarios, a concern identified by the SFI Project Manager S. Buckland for the datasets used in this study (personal communication 16th August 2022). This highlights again the importance of carefully considering the advantages and disadvantages in the selection criteria in terms of data variables, weather conditions and flood stage.

4.5.5. Ground Truth Data

A lack of reliable ground truth records complicated the accuracy assessment process. Consultation with the SFI at an early stage in the development of the NFM project would have been ideal. The value of reliable records of known flood extent on particular dates for accuracy assessment could have provided a pool of sample data for ground truth verification of the flood detection methodology. The benefits of remote sensing for NFM installations therefore needs to be promoted more widely for incorporation into overall project design.

The lack of flood records of stakeholders was surprising. Unfortunately for this study, the excellent records of flood extent on the River Uck by the local media in Uckfield proved to be unsuitable, due to being mainly in an urban environment. This experience though has demonstrated the benefits of contacting local stakeholders, where their own experiences may provide a lead in acquiring suitable ground truth data. In this case, drone footage on YouTube provided the best records from which flood delineation could be verified.

4.5.6. Evaluation Criteria

A fundamental aspect of the study design was the use of data that represented the most challenging circumstances in which to evaluate the NFM installation. What must be considered, is that the measures are not being assessed in a high-flow scenario that may result in low-scale, but frequent flooding. These are some of the most extreme flood events experienced in the last decade for this particular catchment area. This was highlighted when the SFI Project Manager S. Buckland challenged the evaluation of Zone 2. It may well be that the study finds pre- and post-NFM flood characteristics to be similar in some instances. However, what the evaluation fails to identify in its design is the difference during average seasonal events, for example when observations by S. Buckland witnessed more intended flood accumulation in the floodplain in this location.

One area that has not been covered by the evaluation criteria is how the temporal nature of flooding may have changed since the NFM installation. This is a fundamental aspect of large-scale flood mapping studies (Gan et al., 2012) (Martinez and Le Toan, 2007). However, the small-scale nature of the SFI project at Cockhaise Brook produces very short temporal peaks, as illustrated with the river

level graphs for both the pre- and post-NFM flood events in Figures 2.3.1 and 2.3.2 respectively (see Methodology section). River levels for both floods receded to periodic averages within 5-6 days. This is a very short window in which to find suitable satellite imagery that can be consistently compared. The lack of commonality between the ascending pre-NFM flood on 10th January 2016 and in its descending phase on 13th January, demonstrates that a temporal comparison would have been problematic for this particular study.

4.6. Other Potential Areas of Evaluation

Recent drought conditions in the UK have demonstrated how NFM measures slow down both surface and ground water drainage in their proximity. This function of NFM installations was also highlighted by the SFI Project Manager S. Buckland (personal communication, 16th August 2022). It would therefore be interesting to increase the scope of the evaluation to include change detection in drought conditions. This offers the opportunity to acquire data in periods of less cloud coverage, thereby providing more suitable circumstances for the use of optical, as well as SAR imagery to analyse soil moisture in the Cockhaise Brook catchment. Data from a seasonally-similar reference date in more benign conditions could then be used to undertake change detection. Replicating this process for both pre- and post-restoration scenarios would provide insight into how NFM measures may also help ameliorate the worst effects of drought in their vicinity.

5. Conclusion

To improve understanding of how nature-based solutions, such as natural flood management can help address the effects of climate change, more evidence from implemented installations needs to be scientifically evaluated. The principles and technology employed in this study propose an evaluation methodology that tests an NFM installation during one of the largest flood events experienced since its inception. The methodology is portable and simplistic in concept, for application to specifically support further improvements in the design of future NFM installations. Ideally, based on the spatial resolution of the Sentinel-1 imagery used in this study, this evaluation methodology is best applied to larger installations. However, the evaluation proves its value for the small-scale floodplain restoration conducted on Cockhaise Brook.

The selection of the SFI project typifies NFM installations and therefore tested the design of this evaluation for future application elsewhere. Whilst the catchment was not large and floods were short in duration, these are not exceptional characteristics. Specific issues, such as the surface water flows included in the flood detection around Cockhaise Mill, will almost certainly be common occurrences for future evaluation work and highlight how consultation on research findings is vital in gaining technical insight that may derive more subjective conclusions. This was how the scorecard was devised and demonstrates how a project-specific approach is required for this element of the evaluation process.

Change detection seeks to condense differences between two datasets down to the variables being analysed, in this case flood size, form and compactness variances since the introduction of NFM measures. Performance of the NFM installation was analysed by identifying the spatial flood pattern for a sizeable inundation scenario, in relation to the brook's seasonally benign state, for comparison with similar circumstances before the measures were introduced.

Accuracy of the methodology has mainly been verified through innovative means, by consulting drone footage of flooding on other local rivers published on the YouTube platform. The Kappa Statistic of 0.484 does invite scepticism as to the accuracy of the detected flood extents. Improvements in the design of the ground truth sites however concluded that more homogenous ground truth sites, better interpretation of dry sites during digitisation and more consistently sized sites would improve accuracy.

Key to the change detection methodology was the selection of appropriate flood events and perceived benign states that were seasonally similar. This was complicated by the timescales between these events, the flood characteristics of high levels for short windows of time that were experienced with Sussex rivers, identifying similar weather conditions and the installation period. These dictated a relatively long period of nearly four years between the pre and post NFM floods that were used. As found in Zone 1, where possible changes in agricultural use may explain larger post-NFM flood accumulation, longer temporal differences between the pre- and post-NFM events introduce more likelihood of land cover changes. This is though a practical issue in dealing with natural processes and how management measures may have been implemented.

In comparing detected flooding for the pre- and post-NFM events, it can be seen how inundated area may have increased since management measures were introduced on Cockhaise Brook. The necessity of using ascending/descending stages rather than the peak for the pre-NFM scenario require a less definitive statement in this regard, as it is difficult to state exactly what the peak flood inundation would have been.

A robust workflow of GIS operations was assembled that can be easily adapted for other flood management evaluations. Robust testing of how polarisation impacts both flood and false positive detection rates has highlighted the benefits of using VH datasets in both calm and windy conditions. Areas of possible improvement have been identified, such as the HAND mask employed in other

similar research (Clement et al., 2018). Future approaches to verify accuracy may well have suitable ground truth records on site that have been incorporated into the NFM project management framework. However, this study has demonstrated how fresh approaches can be used to source suitable references to verify accuracy.

The evaluation framework can be flexibly adapted to suit the aims and objectives of the flood management scheme being assessed, as well as take account of specific observations coming from stakeholders. In this study, the AOI was broken down into functional zones in which tangible changes could be identified and valued as to the intended design outcomes. A scorecard provided a summary of these flood pattern changes that sought to encapsulate the overall benefits identified in how flooding is now managed in the AOI. Consideration also needs to be taken of how the most challenging events have been used to evaluate the installation. Here, the observations of the SFI Project Manager highlight this point and pose how the evaluation design may need to take account of more frequent events. The challenge is to ensure this does not impact on the portability and accessibility that is at the heart of the design used in this study.

These study results demonstrate clearly how Cockhaise Brook has changed during a serious flood event since the NFM installation. Immediately up and downstream of the main scrapes, mapping from the change detection process has highlighted a reduction in flood extent. These scrapes have doubled rates of flood water accumulation. A desirable effect for Cockhaise Brook has been how these intended increases in flooding have been managed to accumulate in the floodplain immediately around the brook. Overall, this greater accumulation of flood water did not result in a greater footprint of flood extent. The consistently positive changes identified in the scorecard demonstrate how the NFM installation has introduced tangible benefits around Cockhaise Brook.

Based on this proposed evaluation methodology, the findings can provide the potential to strengthen the evidence base for NFM solutions, as part of a wider nature-based approach, to be more seriously considered in responses to adapting infrastructure to the challenges posed by climate change.

6. Bibliography

BERNHARDT, E. S., PALMER, M. A., ALLAN, J. D., ALEXANDER, G., BARNAS, K., BROOKS, S., CARR, J., CLAYTON, S., DAHM, C., FOLLSTAD-SHAH, J., GALAT, D., GLOSS, S., GOODWIN, P., HART, D., HASSETT, B., JENKINSON, R., KATZ, S., KONDOLF, G. M., LAKE, P. S., LAVE, R., MEYER, J. L., O'DONNELL, T. K., PAGANO, L., POWELL, B. & SUDDUTH, E. 2005. Synthesizing U.S. River Restoration Efforts. *Science,* 308**,** 636-637.

BIORESITA, F., PUISSANT, A., STUMPF, A. & MALET, J.-P. 2018. A Method for Automatic and Rapid Mapping of Water Surfaces from Sentinel-1 Imagery. *Remote Sensing,* 10.

BRIVIO, P. A., COLOMBO, R., MAGGI, M. & TOMASONI, R. 2002. Integration of remote sensing data and GIS for accurate mapping of flooded areas. *International Journal of Remote Sensing,* 23**,** 429-441.

CARREÑO CONDE, F. & DE MATA MUÑOZ, M. 2019. Flood Monitoring Based on the Study of Sentinel-1 SAR Images: The Ebro River Case Study. *Water,* 11**,** 2454.

CIAN, F., MARCONCINI, M. & CECCATO, P. 2018. Normalized Difference Flood Index for rapid flood mapping: Taking advantage of EO big data. *Remote Sensing of Environment,* 209**,** 712-730.

CIHLAR, J., PULTZ, T. J. & GRAY, A. L. 1992. Change detection with synthetic aperture radar. *International Journal of Remote Sensing,* 13**,** 401-414.

CLEMENT, M. A., KILSBY, C. G. & MOORE, P. 2018. Multi-temporal synthetic aperture radar flood mapping using change detection. *Journal of Flood Risk Management,* 11**,** 152-168.

ENVIRONMENT AGENCY 2018. Working with Natural Processes – Evidence Directory. Bristol, UK.

ENVIRONMENT AGENCY 2020. National Flood and Coastal Erosion Risk Management Strategy for England. *In:* AGENCY, E. (ed.).

GAN, T. Y., ZUNIC, F., KUO, C. C. & STROBL, T. 2012. Flood mapping of Danube River at Romania using single and multi-date ERS2-SAR images. *International Journal of Applied Earth Observation and Geoinformation,* 18**,** 69-81.

GREEN, K., KEMPKA, D. & LACKEY, L. 1994. Using remote sensing to detect and monitor land-cover and land-use change. *Photogrammetric Engineering and Remote Sensing,* 60**,** 331-337.

HM GOVERNMENT 2018. A Green Future: Our 25 Year Plan to Improve the Environment. *In:* DEFRA (ed.). London.

HUANG, C., CHEN, Y., ZHANG, S. & WU, J. 2018. Detecting, Extracting, and Monitoring Surface Water From Space Using Optical Sensors: A Review. *Reviews of Geophysics,* 56**,** 333-360.

IACOB, O., ROWAN, J., BROWN, I. & ELLIS, C. 2014. Evaluating wider benefits of natural flood management strategies: An ecosystem-based adaptation perspective. *Hydrology Research*.

KASISCHKE, E. S., MELACK, J. M. & CRAIG DOBSON, M. 1997. The use of imaging radars for ecological applications—A review. *Remote Sensing of Environment,* 59**,** 141-156.

KLEMAS, V. 2015. Remote Sensing of Floods and Flood-Prone Areas: An Overview. *Journal of Coastal Research,* 31**,** 1005-1013.

KUMAR, P., DEBELE, S. E., SAHANI, J., RAWAT, N., MARTI-CARDONA, B., ALFIERI, S. M., BASU, B., BASU, A. S., BOWYER, P., CHARIZOPOULOS, N., JAAKKO, J., LOUPIS, M., MENENTI, M., MICKOVSKI, S. B., PFEIFFER, J., PILLA, F., PRÖLL, J., PULVIRENTI, B., RUTZINGER, M., SANNIGRAHI, S., SPYROU, C., TUOMENVIRTA, H., VOJINOVIC, Z. & ZIEHER, T. 2021. An overview of monitoring methods for assessing the performance of nature-based solutions against natural hazards. *Earth-Science Reviews,* 217**,** 103603.

LIANG, J. & LIU, D. 2020. A local thresholding approach to flood water delineation using Sentinel-1 SAR imagery. *ISPRS Journal of Photogrammetry & Remote Sensing,* 159**,** 63.

LONG, S., FATOYINBO, T. E. & POLICELLI, F. 2014. Flood extent mapping for Namibia using change detection and thresholding with SAR. *Environmental Research Letters,* 9**,** 035002.

LU, D., MAUSEL, P., BRONDÍZIO, E. & MORAN, E. 2004. Change detection techniques. *International Journal of Remote Sensing,* 25**,** 2365-2401.

MACLEOD, R. D. & CONGALTON, R. G. 1998. A Quantitative Comparison of Change-Detection Algorithms for Monitoring Eelgrass from Remotely Sensed Data. *Photogrammetric Engineering & Remote Sensing,* 64**,** 207-216.

MANJUSREE, P., PRASANNA KUMAR, L., BHATT, C. M., RAO, G. S. & BHANUMURTHY, V. 2012. Optimization of threshold ranges for rapid flood inundation mapping by evaluating backscatter profiles of high incidence angle SAR images. *International Journal of Disaster Risk Science,* 3**,** 113-122.

MARTINEZ, J.-M. & LE TOAN, T. 2007. Mapping of flood dynamics and spatial distribution of vegetation in the Amazon floodplain using multitemporal SAR data. *Remote Sensing of Environment,* 108**,** 209-223.

MARTINIS, S. & RIEKE, C. 2015. Backscatter Analysis Using Multi-Temporal and Multi-Frequency SAR Data in the Context of Flood Mapping at River Saale, Germany. *Remote Sensing,* 7**,** 7732-7752.

MARTINIS, S., TWELE, A. & VOIGT, S. 2009. Towards operational near real-time flood detection using a split-based automatic thresholding procedure on high resolution TerraSAR-X data. *Natural hazards and earth system sciences,* 9**,** 314.

MATGEN, P., HOSTACHE, R., SCHUMANN, G., PFISTER, L., HOFFMANN, L. & SAVENIJE, H. H. G. 2011. Towards an automated SAR-based flood monitoring system: Lessons learned from two case studies. *Physics and Chemistry of the Earth, Parts A/B/C,* 36**,** 241-252.

MUNYATI, C. 2000. Wetland change detection on the Kafue Flats, Zambia, by classification of a multitemporal remote sensing image dataset. *International Journal of Remote Sensing,* 21**,** 1787-1806.

SCHLAFFER, S., MATGEN, P., HOLLAUS, M. & WAGNER, W. 2015. Flood detection from multi-temporal SAR data using harmonic analysis and change detection. *International Journal of Applied Earth Observation and Geoinformation,* 38**,** 15-24.

SENTHILNATH, J., SHENOY, H. V., RAJENDRA, R., OMKAR, S. N., MANI, V. & DIWAKAR, P. G. 2013. Integration of speckle de-noising and image segmentation using synthetic aperture radar image for flood extent extraction. *Journal of Earth System Science,* 122**,** 572.

SFI, S. F. I. 2022. Natural Flood Management Project End of Year Report 2021/22.

SINGH, A. 1989. Review Article Digital change detection techniques using remotely-sensed data. *International Journal of Remote Sensing,* 10**,** 989-1003.

VAN REES, C. B., NASLUND, L., HERNANDEZ-ABRAMS, D. D., MCKAY, S. K., WOODSON, C. B., ROSEMOND, A., MCFALL, B., ALTMAN, S. & WENGER, S. J. 2022. A strategic monitoring approach for learning to improve natural infrastructure. *Science of The Total Environment,* 832**,** 155078.

XU, H. 2006. Modification of normalised difference water index (NDWI) to enhance open water features in remotely sensed imagery. *International Journal of Remote Sensing,* 27**,** 3025-3033.

ZHANG, B., WDOWINSKI, S. & GANN, D. 2022. Space-Based Detection of Significant Water-Depth Increase Induced by Hurricane Irma in the Everglades Wetlands Using Sentinel-1 SAR Backscatter Observations. *Remote Sensing,* 14**,** 1415.

ZHOU, Y., DONG, J., XIAO, X., XIAO, T., YANG, Z., ZHAO, G., ZOU, Z. & QIN, Y. 2017. Open Surface Water Mapping Algorithms: A Comparison of Water-Related Spectral Indices and Sensors. *Water,* 9**,** 256.